IMPACT RESPONSE OF POLYURETHANE

By

JOHN ANDREW BRYSON

A thesis submitted in partial fulfillment of
The requirements for the degree of

MASTERS OF SCIENCE IN MECHANICAL ENGINEERING

WASHINGTON STATE UNIVERSITY
School of Mechanical and Materials Engineering

DECEMBER 2009

To the Faculty of Washington State University:

The members of the Committee appointed to examine the thesis of JOHN ANDREW BRYSON find it satisfactory and recommend that it be accepted.

_____

Lloyd V. Smith, Ph.D., Chair

_____

Jow-Lain Ding, Ph.D.

_____

David P. Field, Ph.D.

Acknowledgments

I would like to thank the many people who have made this work possible. First I would like to thank my wife Kelie she has been a great support to me. I would also like to thank my advisor Dr Lloyd V. Smith for his guidance and knowledge. Warren Faber has also been a great help to me in supplying the finite element data and figures for this thesis.

IMPACT RESPONSE OF POLYURETHANE

Abstract

By John Andrew Bryson, M.S.
Washington State University
December 2009

Chair: Lloyd V. Smith

The properties of polyurethane, the primary component of softballs, have been found to be rate sensitive. The impact response of softballs containing different rebound properties and stiffnesses were desired. Samples from five different softball models were tested at high and low strain rates.

To test the polyurethane at high strain rates a split Hopkinson pressure bar with aluminum bars was designed and constructed. For comparison the polyurethane materials were also measured at low strain rates of 0.3 s^{-1} on a universal testing machine. An elastic modulus was measured during both the high strain rate and low strain rate tests. A viscoelastic model, obtained from numeric simulations, was compare to the measured high strain rate properties of the polyurethane.

It was found that during impact a softball experiences a peak strain rate of 2500 s^{-1} and strain magnitude of 0.2 strain. The average strain rate in the pressure bar tests was 2780 s^{-1}. The stress measured at 0.2 strain increased 42% when the strain rate increased from 0.3 s^{-1} to 2780 s^{-1}. On average the modulus was 33% high at 2780 s^{-1} compared to 0.3 s^{-1}.The average modulus increase from the increase in strain rate was 33%. The

viscoelastic model predicted stresses three times higher than the stresses observed during the high strain rate tests.

Softballs with different stiffness and rebound properties were compared. The stress and modulus increased with ball stiffness in both the high strain rate and low strain rate tests.

Hysteresis in the load-displacement response from the 0.3 s-1 tests was not sensitive to the measured ball COR. This suggests that rate effects are important to correctly characterize the ball.

Table of Contents

List of Tables

List of Figures

1 Introduction

1.1 Introduction

The behavior of sport equipment is of great interest to those designing and using the equipment. Many sports have impacts that produce stresses and deformations in the materials. In the case of impacts the stress and deformation happens very quickly resulting in high strain rates. Knowing how these materials behave is crucial to improving and understanding sport equipment.

One area of interest is that of softballs. In slow-pitch softball the relative bat-ball speed can be 110 mph. The impact of the bat and ball causes rapid deformation in both the bat and the ball.

To further understand the bat and ball interaction, finite element models have been created to describe this interaction. Softball models have been calibrated to predict behavior of the bat-ball interaction at 110 mph. While the performance predictions are generally in good agreement with experiment, the force displacement curve of the softball and FEA model don't match up. The models don't do a very good job of matching bat-ball interaction at other speeds (1). The model predicts a stiffer ball than is seen in actual testing as shown in figure 1.1. To obtain a better model more accurate properties of the softball are needed.

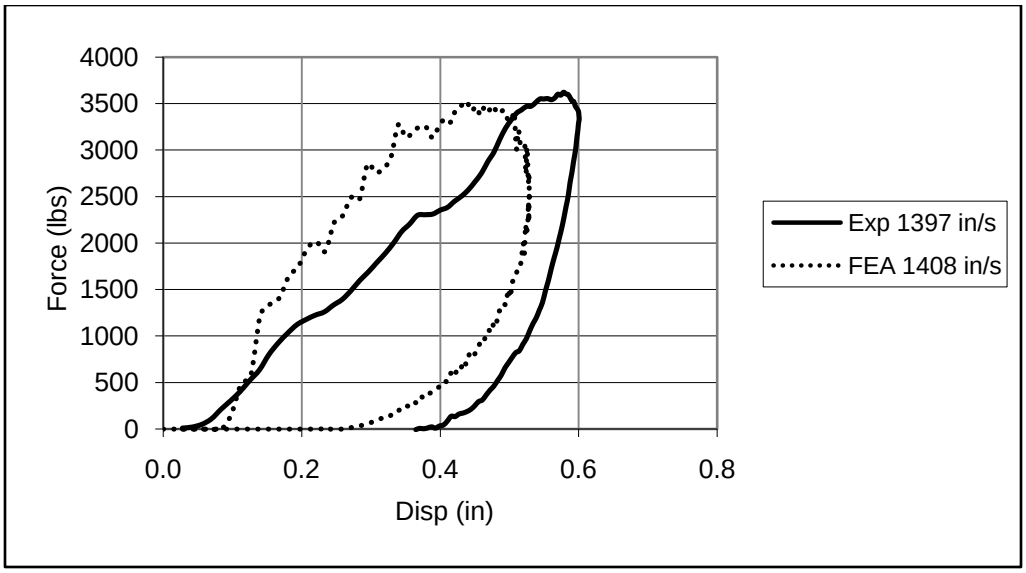

Figure 1.1 Force Displacement of Softball and FEA Model

Properties of polymeric materials are often dependent on the rate of strain. It has been observed that this is the case with softballs. The conventional way of measuring stress-strain response is with a universal testing machine, which can achieve strain rates up to 10 s^{-1}. The strain rate that is observed in a softball collision is much higher with calculated strain rates at 2500 s^{-1} (2). A method is needed to measure the higher strain rate properties of the softball.

The typical softball is constructed from a polymeric center or core with a leather or synthetic cover. A cross-section of a softball is shown in figure 1.2. The most common polymer used in the softball core is polyurethane. The majority of the ball's behavior is due to the response of the polyurethane core. A Split-Hopkinson pressure bar (SHPB) was built to measure the properties of the polymeric core at high strain rates to compare softballs with different stiffness and rebound properties.

Figure 1.2 Softball Cross-Section

2 Background

2.1 Introduction

There is an ever growing need to understand how materials behave. An increased understanding of the materials allows the materials to be implemented efficiently and effectively in designs. Laboratory testing is needed to increase the understanding of materials. With the understanding obtained in the laboratory the applications using those materials can be designed better.

There are several things that can affect a material's performance including temperature, environment, and strain rate. When a material is used in an application that can sustain high strain rates it is important to know the properties at those higher strain rates. The Split-Hopkinson Pressure Bar (SHPB) is a common way of testing materials at high strain rates (3).

The background of the SHPB as well as the setup and how it works is discussed in this chapter.

2.2 Physical Setup

2.2.1 Introduction

The Split Hopkinson Pressure bar consists of two bars of the same diameter. The bars are aligned axially to ensure linear stress wave propagation. The bars are mounted to allow longitudinal movement but constrained in the transverse direction. This can be done with the use of linear bearings. To insure accurate readings the bars need to be

straight, aligned, and free to move axially (3). A sketch of a typical SHPB bar setup is shown in figure 2.1.

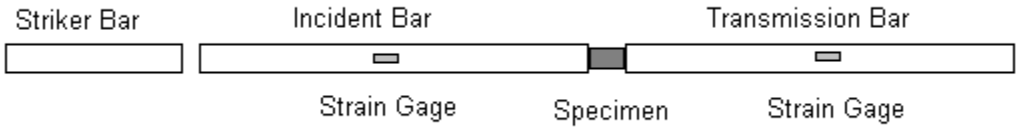

Figure 2.1 Split Hopkinson Pressure Bar Setup

To create a compression wave a striker bar is fired at the incident bar often called the input bar. Compressed air is used to fire the striker bar often using an accumulation tank attached to a regulator fed by a supply line. Figure 2.2 shows the theoretical strain history of the strain gages. The compression wave created by the striker bar will travel down the incident bar to the sample where it is partially reflected and transmitted through the specimen. The signal transmitted though the specimen enters the transmission bar often called the output bar. At the other end of the transmission bar is often a momentum trap used to reduce the movement of the bars.

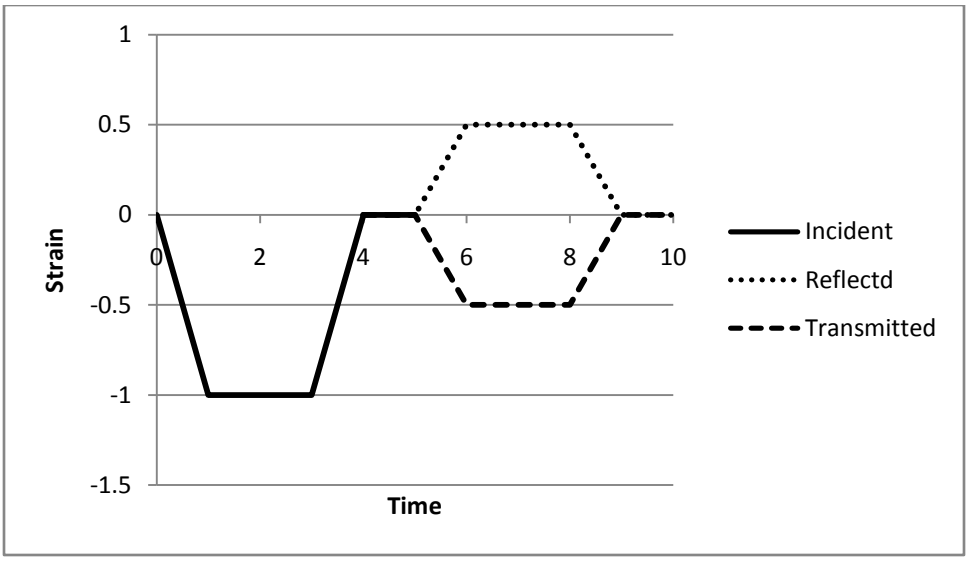

Figure 2.2 Theoretical Strain Gage History

The compression wave in the SHPB can be adjusted with the length or velocity of the striker bar (3). The increased length corresponds to an increased signal duration, and an increased velocity corresponds to an increased strain rate. These two parameters can be adjusted to attain the desired conditions.

The length of the striker bar is limited by the length of the incident and transmission bars, also known as the pressure bars. The striker bar can be no greater than half the length of the pressure bars. This is because for data reduction there can't be overlap between the incident wave and the reflected wave. The length of the incident bar limits the length of the compression wave. The longest compression wave that can be measured is half the length of the incident bar. To adjust for some of these limitations some investigators have varied the lengths of the incident and transmission bars so that the incident bar is longer than the transmission bar (3; 4).

2.2.2 Instrumentation

Since the SHPB was first investigated there have been many different ways of measuring the stains in the pressure bars. Kolsky used a capacitance instrumentation to measure the properties in his first pressure bar (5). The most common way of measuring the strain in the pressure bars is with strain gages (3).

There have been other ways of obtaining the material properties other than strain gages. Some investigators have used transducers to measure the force and acceleration at the sample boundaries (6). This allowed the investigator to use pressure bars made of non-linear elastic materials. In this setup the transducers are close to the specimen, and the forces that the transducers read are the forces the specimen is subjected to. With a traditional strain gage at the center of non-linear elastic bars non-linear wave propagation would have to be applied. Another method is to use quartz crystals close to the sample to measure the forces on either side of the sample (7). This has been done to check for a uniform stress distribution within the specimen.

There are different setups of strain gages that investigators have used. Depending on the setup and what the investigator is interested in, it is common to see a quarter bridge as well as a half bridge setups. The quarter bridge setup uses one strain gage. The half bridge setup uses two strain gages on opposite sides of the bar. The half bridge setup can be used for subtracting off the effects of bending. If the bars are straight and aligned properly there should not be any bending so the quarter bridge setup should be sufficient.

In order to read the strain gage signals the signal needs to be amplified. There are many different amplifiers used by investigators. It is important to have an amplifier that

has a sufficient frequency response since the experiment happens over a very short period of time. It was found that a frequency response of 160 kHz at -3db was sufficient. The amplifiers are then attached to a device used to read or display the signal. Some common devices for displaying the signals are oscilloscopes and computers (3).

2.2.3 Equations

Once the signals have been captured the data needs to be reduced. A typical strain history of a split Hopkinson pressure bar is shown in figure 2.3. There are three waves that are recorded, the incident, reflected, and transmitted waves. The first and second waves recorded on the incident bar are the incident and reflected waves respectively. The first wave recorded on the transmission bar is the transmitted wave.

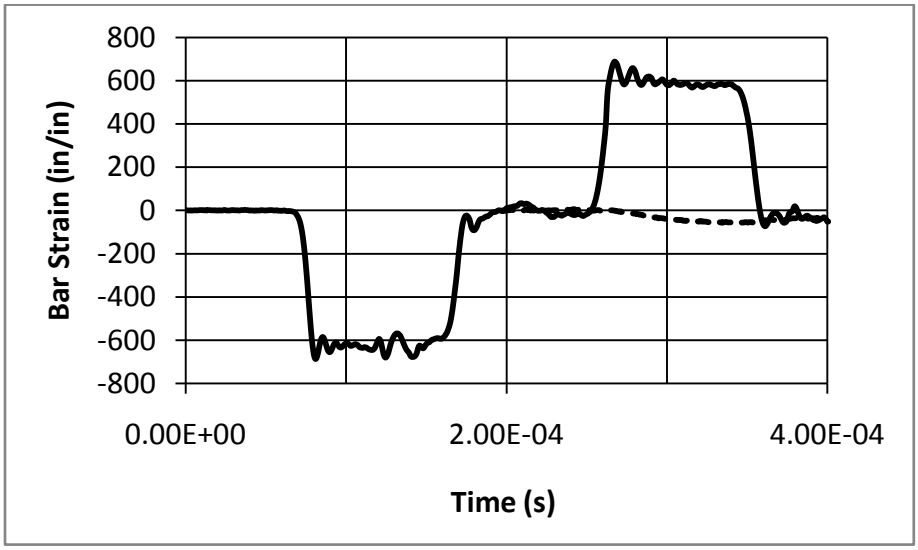

Figure 2.3 SPHB Strain Gage Readings of Polyurethane Sample (solid: incident bar, dashed: transmission bar)

The incident wave is the pulse that is induced by the striker bar. This pulse then travels down the bar and is partly reflected and transmitted into the specimen. As the

transmitted pulse travels through the specimen it deforms the specimen. The transmitted pulse then progresses into the transmission bar (3).

From the incident, reflected and transmitted strain waves the specimen stress, strain, and strain rate can be calculated. There are several ways to develop the equations for the split Hopkinson pressure bar. One way is to look at the forces on an element in the specimen (8). Another way is to start from the wave equation (3). In this development the latter will be shown.

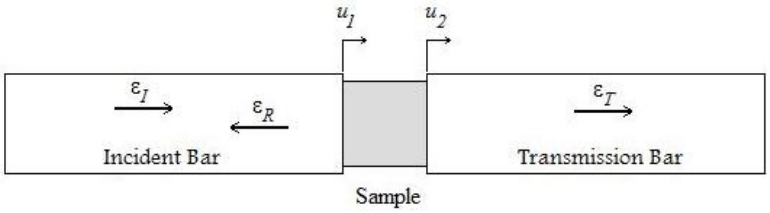

Figure 2.4 Wave Directions in a SHPB

The wave equation is

$$\frac{\partial^2 u}{\partial x^2} = \frac{1}{C_o}\frac{\partial^2 u}{\partial t^2}, \qquad 2.1$$

where C_o is the wave speed and u is the displacement. The solution to the wave equation can be written as the sum of two waves, as

$$u_1 = f(x - C_o t) + g(x + C_o t) = u_I + u_R \qquad 2.2$$

for the incident bar and as

$$u_2 = h(x - C_o t) = u_T \qquad 2.3$$

for the transmission bar. The subscripts I, R and T refer to the incident, reflected, and transmitted waves respectively.

One dimensional strain is given by

$$\varepsilon = \frac{\partial u}{\partial x}. \qquad 2.4$$

Applying this relation to equation 2.2 strain in the incident bar can be expressed as

$$\varepsilon = f' + g' = \varepsilon_I + \varepsilon_R. \qquad 2.5$$

It can be shown that the time derivative of equation 2.2 leads to

$$\dot{u}_1 = C_o(-f' + g') = C_o(-\varepsilon_I + \varepsilon_R). \qquad 2.6$$

Performing a similar step with equation 2.3 gives

$$\dot{u}_2 = -C_o\varepsilon_T. \qquad 2.7$$

Since equations 2.6 and 2.7 are true for all location in the incident and transmission bars respectively they are true for the surfaces contacting the specimen. Combining these equations and calculating strain by dividing by L the un-deformed specimen length gives the specimen strain rate as

$$\dot{\varepsilon} = \frac{(\dot{u}_1 - \dot{u}_2)}{L}. \qquad 2.8$$

Substituting equations 2.6 and 2.7 into equation 2.8 results in

$$\dot{\varepsilon} = -\frac{C_o}{L}(\varepsilon_I - \varepsilon_R - \varepsilon_T). \qquad 2.9$$

Using Hook's Law and the definition of compressive stress

$$\sigma = \frac{F}{A} = E\varepsilon, \qquad 2.10$$

the force at each end of the specimen can be written as

$$F_1 = AE(\varepsilon_I + \varepsilon_R) \qquad 2.\ 11$$

and

$$F_2 = AE\varepsilon_T \qquad 2.\ 12$$

where A and E are the bar cross-sectional area and modulus of elasticity. Equations 2.11 and 2.12 assume the incident and transmission bars have the same cross-sectional area as well as elastic modulus.

When the specimen is in equilibrium the forces on each side of the specimen are the same. Assuming the specimen is in equilibrium equation 2.11 and 2.12 are equal and it follows that the transmitted strain is equal to the sum of the incident and reflected strain histories shown as

$$\varepsilon_T = (\varepsilon_I + \varepsilon_R)\,. \qquad 2.\ 13$$

Using the relation for the strains shown in equation 2.13, the strain rate in equation 2.9 becomes

$$\dot{\varepsilon}(t) = \frac{2C_o}{L}\varepsilon_R(t)\,, \qquad 2.\ 14$$

which is the strain rate in the specimen. Integrating this equation will yield the strain in the specimen as

$$\varepsilon(t) = \frac{2C_o}{L}\int_0^t \varepsilon_R(\tau)d\tau\,. \qquad 2.\ 15$$

The stress in the specimen can be obtained by dividing the force in equation 2.12 by the specimen cross-sectional area expressed as

$$\sigma(t) = \frac{A}{A_s} E\varepsilon_T(t) \quad . \qquad 2.16$$

The term A_s is the specimen cross-sectional area and A and E are the bar cross-sectional area and modulus respectively. For the strain and stain-rate the wave speed C_o can be calculated as

$$C_o = \sqrt{\frac{E}{\rho}} \quad , \qquad 2.17$$

where ρ and E are the pressure bar mass density and modulus respectively.

These equations are based on the assumption that the forces at both ends of the specimen are the same. In the case of soft materials this is not always true. Softer materials tend to have slower wave speeds requiring a longer period of time for both sides to be in equilibrium. With longer soft materials the specimen can't achieve equilibrium within the short time the stress is applied. Investigators have tried different methods for insuring that the specimen is in equilibrium (4; 7; 9; 10; 11). It has been noted that with thicker samples it takes longer for the sample to obtain stress equilibrium, so thinner samples are often used.

Many soft materials and foams do not have constant volume under deformation. This makes it difficult to find the true stress and true strain. Because of this engineering

stress and strain are used in this thesis. The stress and strain obtained from equation 2.15 and 2.16 are engineering stress and strain respectively.

2.3 Split Hopkinson Pressure Bar History

The first person to do work with pressure waves in bars was Bertam Hopkinson in 1914 (12). Hopkinson used a single bar with a sample fixed to the end of the bar using grease. This bar assembly was suspended on two strings allowing it to swing. A projectile was fired at the end of the bar using explosives. This impact created a compressive wave that traveled down the bar. At the opposite end of the bar was a sample attached to the bar with grease. The compressive wave would reach the end of the sample and as the wave was being reflected at the end, some of the momentum would be trapped in the sample causing it to fly off.

By varying the size of the sample and length of the compressive wave Hopkinson could tune the bar so that all of the energy was transferred into the sample. He was able to measure the energy remaining in the bar by suspending it on two strings and measuring the pendulum swing of the bar assembly. The sample's momentum was measured using ballistics jelly. The momentum could be determined by the distance the specimen was projected into the jelly.

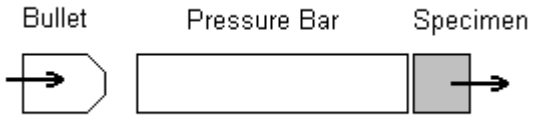

Figure 2.5 Hopkinson's Bar Setup

In 1949 Henry Kolsky developed what is now called the Split-Hopkinson Pressure Bar or some call it the Kolsky bar (5). Kolsky used two bars in series with a thin sample sandwiched in between. A projectile was fired into the first bar using explosives. He used capacitance instrumentation to measure the deflection of the bars. For the incident bar he measured the transverse deflection with a rod perpendicular to the bar. The transmission bar's deflection was measured at the end of the bar with a rod. The rod was attached to one end of a capacitance plate. The capacitance of the plate would change as the distance between the plates changed. Kolsk related the change in capacitance to the displacement on the bars.

Using this deflection he calculated the strain in each of the bars by using linear wave propagation theory similar to that in equations 2.14-2.16. He was able to measure the high strain rate properties of several materials including rubber, copper, lead and others.

Since Kolsky developed the Split-Hopkinson Pressure bar there have been many improvements. Lindholm and Yeakley made alterations to the split-Hopkinson pressure bar in order to test materials in tension as well as compression (13). In 1988 Khan and Hsiao measured plastic waves in solids using resistance foil stain gages (14). The use of strain gages to measure the strains in SHPBs has become quite efficient.

Many different materials have been characterized at high strain rates. Chou, et al. investigated the high strain rate properties of different plastics including Nylon 6/6 (15). They were looking at the temperature increase during high strain rate testing using

imbedded sensors for the temperature. A SHPB was used to test the plastics at high strain rates by Chou.

There has been some work done in testing of soft materials. Chen, et al. has done a lot of work testing soft materials (7). Chen, et al. also tested polyurethane with a SHPB (4). In that investigation they were interested in the effect that density had on the high strain rate behavior of polyurethane.

There are a few challenges that are associated with testing soft materials. These challenges are discussed in section 2.4. An overview of different techniques for testing soft materials was written by Song, et al. (10).

More sophisticated computers for the numerical analysis are now available to investigators as well as better strain gages and faster signal conditioners. The SHPB has become the most popular form of testing the behavior of materials at high strain rates.

2.4 Soft Materials SHPB Testing

2.4.1 Introduction

There has been quite a bit of interest in testing soft materials at high strain rates. A lot of the interest is based on the increased use of soft materials in modern applications. Often these soft materials are used in applications where the strain rate is quite high or could be high in the case of an impact, for instance automobile safety equipment, aerospace, sporting good applications, and much more. A good understanding and accurate models are needed when designing applications that use these materials.

2.4.2 Problems Associated with Soft Material SHPB Testing

There are several techniques for characterizing soft materials the most common being a Split-Hopkinson pressure bar. The SHPB allows the investigator to attain the desired high strain rates. But there are several problems that are associated with testing soft materials using a traditional SHPB.

There are two main problems encountered with testing soft materials with a split Hopkinson pressure bar. The first is that the magnitude of the transmitted wave is small and often difficult to distinguish from the base line electrical noise. Second, the elastic impedance of a soft material is very low, which means that the velocity of the elastic wave generated from the pressure bar travels much more slowly in the sample than the bar. Third, the sample must be in a state of uniform stress for the reduction equations to apply. Because of the low impedance and the soft characteristics of the material a uniform stress may be difficult to obtain (3).

These problems need to be addressed in order to obtain accurate data. There are several ways to mitigate some of these problems. Many of the methods have advantages and disadvantages.

2.4.3 Signal to Noise Ratio

Low magnitude transmitted waves are often seen in SHPB testing of soft materials. The problem with low magnitude transmitted signals is that the signal to noise ratio can be so low that the signal is indistinguishable from the base line noise. There are several things that investigators have done to increase the signal to noise ratio. Besides

changing sample geometry most of the other techniques fall into two categories, changing the pressure bar material and, changing the bar geometry.

Using a pressure bar with lower impedance can reduce the impedance mismatch between the bar and the sample. It is best to have a bar material that has an impedance that closely matches that of the sample. Reducing the impedance mismatch can allow a larger signal to be transmitted through the sample.

Some of the lower impedance materials that are used are, titanium-alloys, aluminum-alloys, magnesium or magnesium-alloys, and polymers (9; 10). As long as the bar material is linear elastic the driving theory behind the Split-Hopkinson pressure bar holds true. In the case of polymeric pressure bars a nonlinear correction needs be used in the reduction of the data (16).

Another approach to finding the properties using a polymeric pressure bar is to use velocity gages (6). In this case the Split-Hopkinson bar was modified with transducers in a magnetic field. Using this method the velocities of the ends of the sample were measured. This makes it possible to measure the behavior of the sample material without using a non-linear correction of the polymeric pressure bars. The problem with this method is that the alignment of the transducers in the magnetic field is critical and large errors can be introduced with misalignment.

Another method for increasing the signal to noise ratio in the transmitted bar is to use a hollow transmission bar (9; 10). Although this helps increase the signal to noise ratio, the change in geometry should be considered when reducing the data. To ensure accurate results a correction for the hollow cylinder should be used. Some critics to this

method argue that the signal does not propagate the same in a pipe as in a cylinder, introducing uncertainty in the readings obtained from this method.

2.4.4 Stress Distribution

Another problem with testing soft materials is the low inherent flow stress. The low inherent flow stress can lead to a non-uniform stress distribution, which can cause the characterization of the material to be inaccurate. The equations and theory behind the SHPBs assumes that the sample has a uniform stress distribution (3).

To ensure that the soft sample is in uniform stress distribution the stress at both sides of the sample can be measured. There are several methods that investigators have used to do this. One method is the use of quartz crystal transducers on either side of the sample (7). The quartz crystal has similar impedance to the aluminum bars that it is in series with. Figure 2.5 shows the small disks on either side of the crystals installed to protect the crystal. These transducers measure the force on either side of the sample. By using pulse shaping techniques the two readings can be matched and a uniform stress distribution obtained.

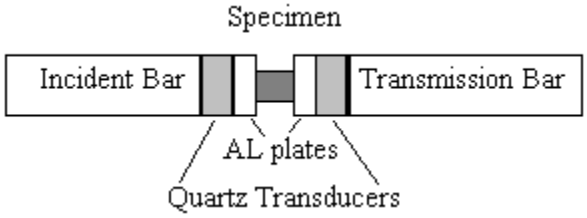

Figure 2.6 Quartz Crystal Transducer Setup

The disadvantage of using the quartz transducers to measure force is that the transducers can disrupt the waves propagating through the bars. The increase in the

number of surfaces the wave is passing through can increase the amount of error generated during a test.

There are other ways of determining if the specimen is in uniform stress distribution. Song and Chen wrote an overview of different techniques for testing soft materials (10). Besides the use of load cells to measure the stress at both end of the specimen, the stress can be calculated using the force on the first face of the specimen. This force is shown in equation 2.11. The incident and reflected waves can be added and used to replace the transmitted wave in equation 2.16. The specimen's uniform stress distribution can be quantified using equation 2.16 and

$$\sigma_1(t) = \frac{A}{A_s} E(\varepsilon_I(t) + \varepsilon_R(t)) \quad 2.18$$

.

Dividing equation 2.16 by equation 2.18 gives the stress equilibrium factor as

$$\sigma_{EQ} = \frac{\sigma_T}{\sigma_I + \sigma_R} \quad 2.19$$

.

Figure 2.7 shows the numerator as σ_2 and the denominator as σ_1. The specimen is said to be in perfect equilibrium when the stress equilibrium factor goes to unity (10).

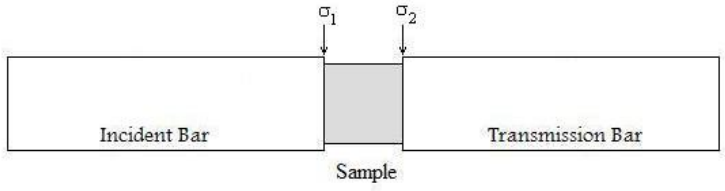

Figure 2.7 Location of Stress for Stress Equilibrium Calculations

The advantage of using the incident and reflected waves to calculate the stress equilibrium is that the SHPB does not have the added complexity of the load cells. The

downside is that when the transmitted wave is small the incident and reflected waves are almost equal in magnitude and opposite in direction. Adding the incident and reflected waves can introduce large amounts of error to the stress calculated.

Another way to reduce the time needed to attain uniform stress distribution is changing sample size. Reducing sample length reduces the time needed to reach uniform stress distribution. One of the effects of reducing sample length is that the strain and strain rate also increase. Depending on what parameters the investigator is interested in this could be beneficial.

2.5 Softball Background

Since softballs are a large focus of this thesis a discussion about the construction of the softball is helpful. There are two factors that were compared in the studies done for this thesis, the stiffness and the rebound properties of the softball.

2.5.1 Softball Properties

The stiffness of softballs can be measured by compressing the softball between two flat plates a 0.25 inch and recording the load. This is referred to as the compression of the softball. The softballs used in this thesis had nominal compression values of 300 lbs, 375 lbs, and 525 lbs. Balls are often sold with a maximum compression displayed on the ball.

Another measure of softballs stiffness is called dynamic stiffness (DS). This is a measure of balls stiffness during a collision with a cylinder. The cylinder has load cells

mounted opposite the collision site used for measuring the impact force. DS can be calculated using the kinetic energy expressed as

$$\frac{1}{2}mv^2 = \frac{1}{2}kx^2, \qquad 2.\ 20$$

where m is the mass of the ball, v is the velocity, and k is the dynamic stiffness. Force can be expressed as

$$F = kx. \qquad 2.\ 21$$

Using these equations the dynamic stiffness k can be expressed as

$$k = \frac{1}{m}\left(\frac{F}{v}\right)^2. \qquad 2.\ 22$$

The velocity is obtained by measuring the velocity before the collision and the force is measured from the load cells.

The rebound properties of the softball are quantified using the coefficient of restitution (COR). The COR is a measure of the energy retained after a collision with possible values ranging from 0 to 1. The softballs used in this thesis had nominal COR values of .40, .44, and .47. Balls are often sold with the nominal COR value displayed on them. The decimal point is often left off.

2.5.2 Softball Construction

The softball is made from a rigid polyurethane foam center wrapped in a cover. The covering is usually made from leather or synthetic and is often white or yellow. Refer to figure 1.2 for a picture of the cross-section. One of the interests of this thesis is to determine the impact properties of the foam center.

Rigid polyurethane foam is made by the reaction of polyisocyanates and polyols in the presence of catalysts, surfactants, and blowing agents (17). The reaction is an exothermic chemical reaction among liquid reactants. By varying the liquid reactants different foam properties can be attained.

There are several different methods for preparing rigid polyurethane foam. The methods are the block and sheet, poured in place, and sprayed. Softballs are made using a poured in place method.

Softballs are constructed by mixing the polyisocyanates and polyols in a large mixing tank. The batter, in the consistency of pancake mix, is poured into the molds and then rotated while it cures. It takes about three minutes to cure. Since the reaction is an exothermic reaction the temperature needs to be monitored while curing. There are several variables that are adjusted to achieve different properties of the softball, cure time, chemical makeup, and temperature (18).

2.5.3 Polyurethane Behavior

It is beneficial to know the expected behavior of polyurethane foam. Work was done on the high strain rate properties of rigid polyurethane foam by Chen, et al. (4). Chen found that polyurethane behaved similar to a structure rather than a solid. As the foam is loaded the structure deforms slightly. Further loading causes the cell walls to buckle and the behavior of the foam changes and becomes much softer until the cells fully collapse, then the material becomes much stiffer again. Chen found that the behavior of the foam and how it deforms through this general cycle is dependent on the

foam's density. Chen's graph for the foam that has a density similar to softball polyurethane foam is shown in figure 2.8.

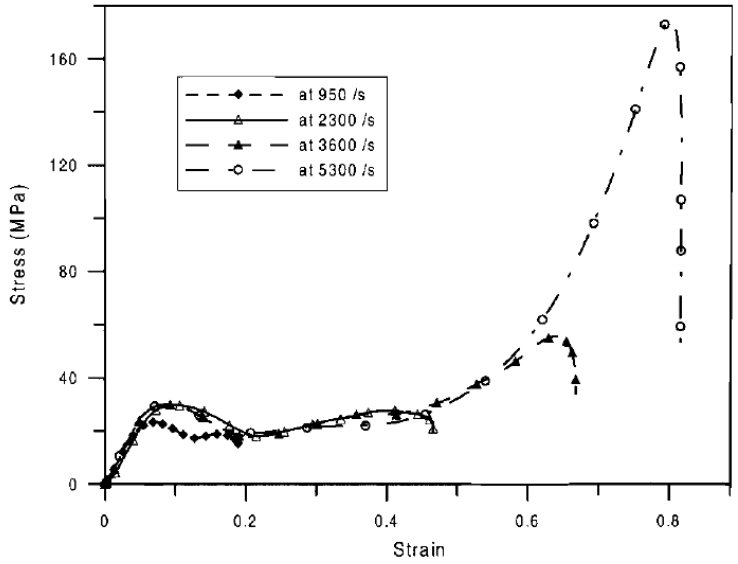

Figure 2.8 Dynamic Compressive Stress-Strain Curves for Polyurethane Foam with a Density of 445 kg/m^3 from Chen

2.6 Summary

Testing materials at high strain rates can be done quite effectively with a split-Hopkinson pressure bar. The SHPB consists of two bars instrumented with strain gages. A striker bar is fired at one end creating a compression wave that travels down the bar and through the sample. These strain waves are read from the strain gages mounted on the pressure bars. From these strain waves the specimen strain rate, strain, and stress can be calculated.

The split-Hopkinson pressure bar was proposed by Kolsky and is an efficient way of measuring the high strain rate properties of materials. There have been many

improvements to the split-Hopkinson pressure bar including resistance strain gages, tension testing, and soft material testing.

There are several problems associated with testing soft materials with a split-Hopkinson pressure bar. The most common problems are the signal to noise ratio and attaining uniform stress distribution. A low signal to noise ratio can make it difficult to obtain a large enough transmitted signal. Also reaching uniform stress distribution can take longer with soft materials. Shortening the specimen length can help reduce the time needed to reach a uniform stress distribution and it can help increase signal to noise ratio.

The coefficient of restitution and compression are common ways of quantifying the behavior of softballs. The COR is a measure of the amount of energy retained after a collision. The compression is a measure of the load needed to compress a softball 0.25 inches. The COR properties investigated for this thesis ranged from .40 to .47. The compression properties ranged from 300 to 525.

3 Apparatus

3.1 Split Hopkinson Pressure Bar Setup

3.1.1 Introduction

The split Hopkinson pressure bar constructed for this project was designed to test soft materials. The construction of the pressure bar is discussed in this section including the structure and frame, instrumentation and electronics, and cannon setup.

3.1.2 Pressure Bar Structure and Frame

The split Hopkinson pressure bar was mounted on a framework constructed out of Bosch tubing. The setup was mounted on a ten foot piece of Bosch 45X90 tubing. This frame is shown in figure 3.1. There were three leg assemblies attached to the structure using ninety degree gussets. Each of these leg assemblies had adjustable feet for leveling the assembly. The cannon and pressure bars were mounted to the Bosch tubing using custom made pillow blocks that have three setscrews for adjusting the alignment, figure 3.2. The cannon and the bars were each secured using two pillow blocks. The pillow blocks used for the bars had polymer bearings to help reduce friction and reduce conductivity to the frame. There was a momentum trap to constrain the motion of the transmission bar consisting of a short two foot bar with a padded block shown in figure 3.3.

Figure 3.1 Split Hopkinson Pressure Bar Setup

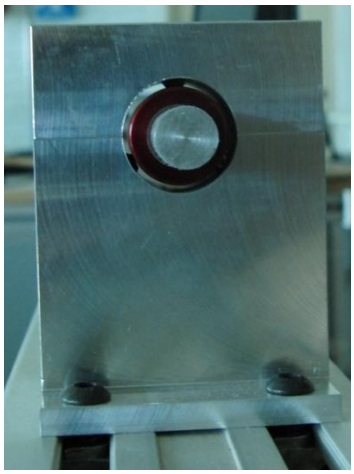

Figure 3.2 Adjustable Pillow Blocks

Figure 3.3 Momentum Trap on Split Hopkinson Pressure Bar

3.1.3 Pressure Bar Electronics

The two bars of the SHPB were three feet long and 0.5 inches in diameter. The bars were made of 6061 aluminum. At the center of each bar aligned with the length were strain gages glued using Vishay Micro Measurements M-Bond 200 adhesive. A picture of a mounted and wired strain gage is shown in figure 3.4. The strain gage was a Vishay Micro Measurements EA-06-062AQ-350/W gage having a resistance of 350 Ohms. From the strain gage there were small wires attached to soldering pads. These strain gages were connected to a conditioner using shielded twisted pair strain gage wire number 326-BSV from Micro Measurements.

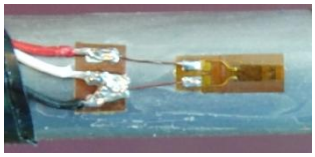

Figure 3.4 Mounted and Wired Strain Gage

The conditioners used were 2310B signal conditioning amplifiers from Vishay Micro-Measurements. These were picked because of the high frequency response of 160 kHz at -3db and 1000 gain. The excitation voltages of the conditioners were set to 10 volts. It was found that 15 volts tended to warm the strain gage causing the strain reading

to creep with time. The conditioners can be seen in figure 3.4. The conditioners were connected to a PC using a connection block SCB-68 made by National Instruments. The connection block was connected to a National Instruments analog-to-digital PCI-6111 board inside a Dell 4600 desk top computer. The NI PCI-6111 board could sample two analog channels simultaneously at 5 mega-samples per second. The connection block used for connecting the instrumentation to the A/D board can be seen in figure 3.5. The A/D converter allowed the strain values from the conditioner to be read and recorded as well as controlling the cannon pressure and valve firing.

Figure 3.5 Signal Conditioners

3.1.4 Cannon Setup

Figure 3.6 is a picture showing the control box setup, and figure 3.7 is a picture showing the cannon setup with the different parts labeled. In order to fire the striker bar the cannon was supplied with compressed air. There was a five gallon accumulation tank that was used to supply the air for firing. The tank pressure was regulated using a digitally controlled SMC regulator ITV3050-31N3CL4 which received input from the PC. Connected to the tank was a MAC valve 57D-32-110AA used for firing the compressed air.

The cannon barrel was attached to the valve using a 0.5 inch high pressure hose. The steel cannon barrel was 24 inches long with a 0.5 inch bore. The MAC valve was fired using a 24 volt signal supplied through a solid state relay. The control box is shown in figure 3.6. In this figure the solid state relay can be seen as well as two power supplies and the connection block.

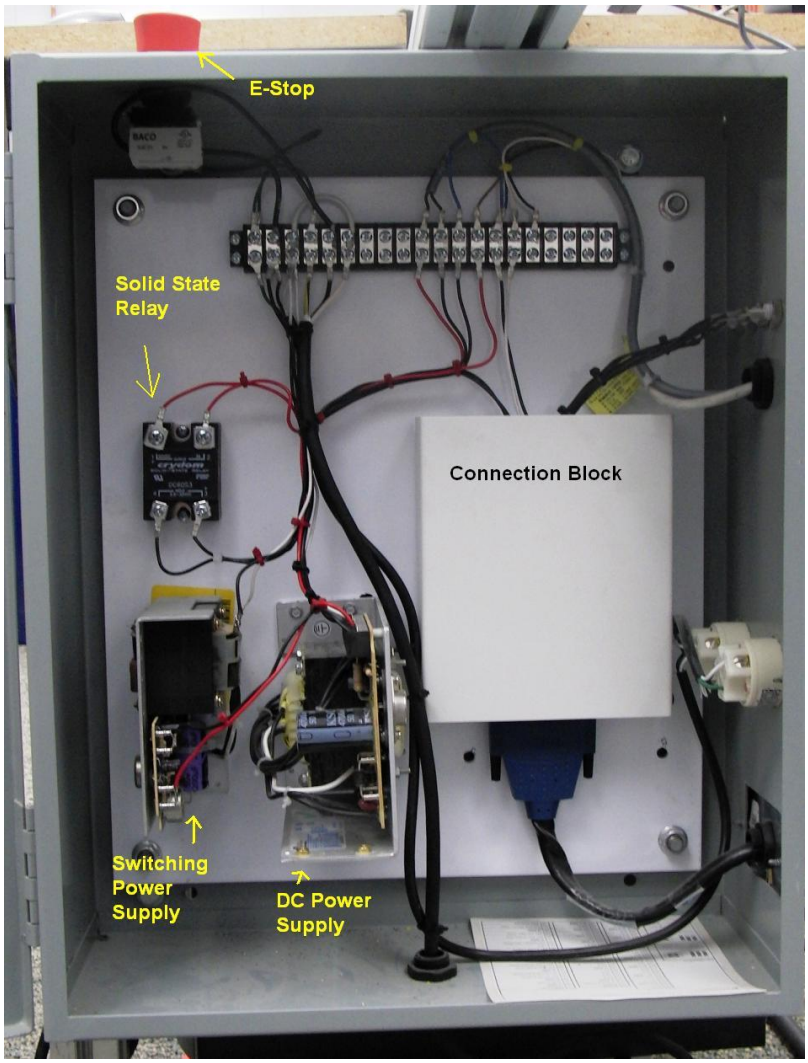

Figure 3.6 Control Box

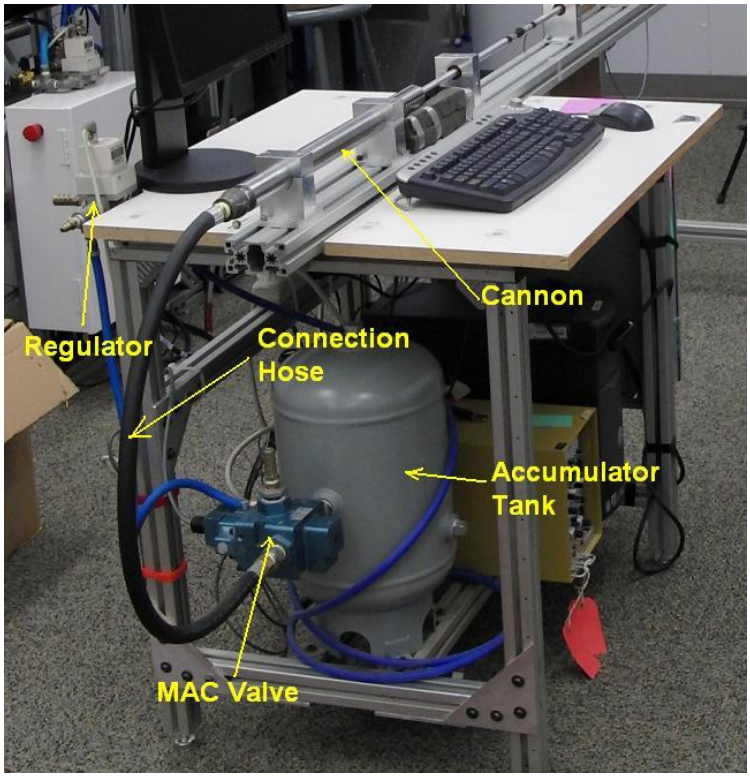

Figure 3.7 Cannon Assembly

3.2 Pressure Bar Operation

The operation of the split Hopkinson pressure bar is fairly simple. A detailed step by step operating procedure can be found in appendix A. The pressure bar is controlled using a LabVIEW vi named “Pressure Bar.vi”. There are several aspects about the pressure bar that can be controlled using this front panel setup. The program is used to save and crop the strain gage data as well as control the cannon pressure and firing. Figure 3.8 shows a screen shot of the front panel setup.

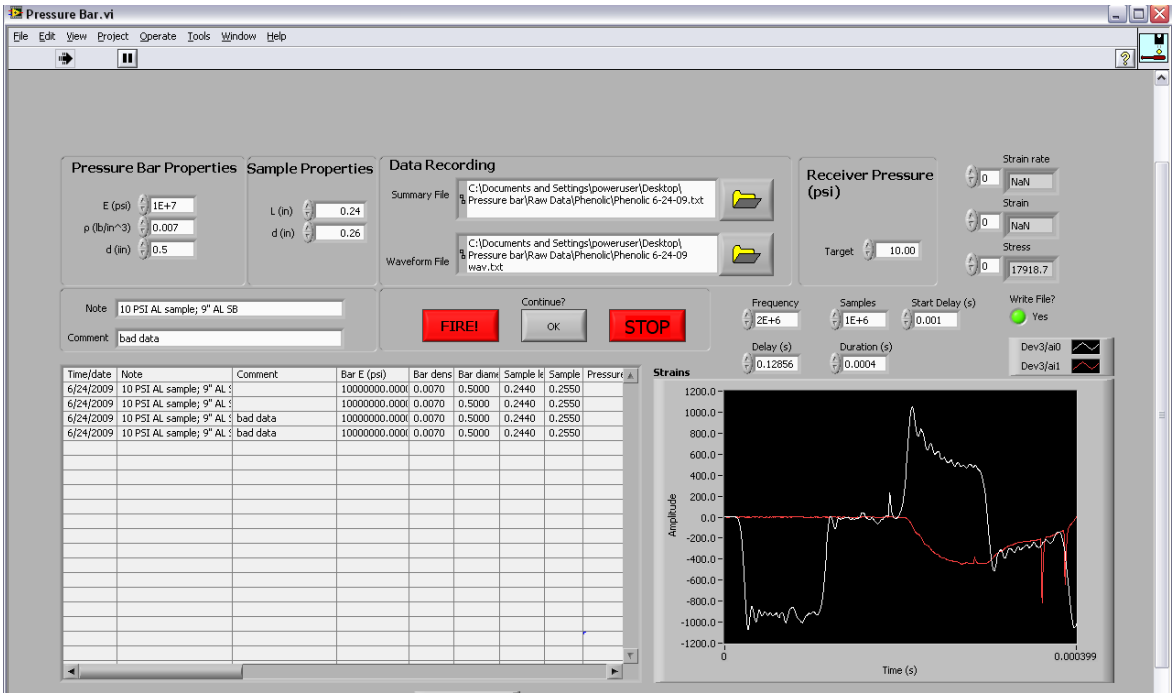

Figure 3.8 Pressure Bar.vi Front Panel

To fire the cannon the specimen bar ends were greased with a small amount of grease and the specimen was placed between the incident and transmission bars. The striker bar was pushed to the breach of the cannon using a small rod. The incident bar was slid so that the end was at the exit of the cannon barrel. It was important to have both bars touching the sample as shown in figure 3.9. When everything was in place the signal conditioners were zeroed and the fire button was pressed in the Pressure Bar.vi front panel.

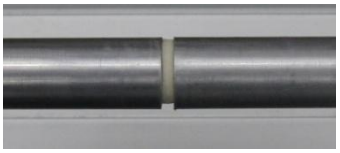

Figure 3.9 Installed Sample in Split Hopkinson Pressure Bar

The data window needed to be adjusted so that the first two waves on the incident bar were visible. The data displayed is the data that is written to the file. Once the data window was adjusted the Ok button was pressed and the data was saved to the file.

3.3 Problems and Solutions

During construction of the SHPB there were several problems that were encountered. This section discusses those problems and some of the steps taken to fix the problems. The two main problems were signal noise and cannon alignment.

3.3.1 Noise Problems

As the SHPB was being debugged there was a fair amount of noise that was observed. Several changes were investigated to reduce the noise, many of which had little effect. The noise problems observed as well as the attempted solutions are discussed below.

One of the first solutions investigated dealt with a grounding issue. There was a poor ground between the electronics and the earth ground. After some investigation it was determined that the supplied power was not connected to an earth ground. This was solved by connecting to an electrical outlet located closer to the source that had a good earth ground. This electrical outlet had been installed recently and complied with current electric standards.

Another noise problem that was observed dealt with a signal spike that was observed when the cannon valve opened and closed. There were several failed attempts to solve this problem. It was determined that the signal spikes did not interfere with the data

that was being investigated. Some of the steps to eliminate or reduce this spike were, the installation of a line snubber, and separating the power supplies to the valve and regulator. The valve was on a switching power supply and the regulator and everything else that needed power was connected to a linear power supply. This is why there are two power supplies shown in figure 3.5.

When the split Hopkinson pressure bar was first built and tested, it was found that the expected trapezoidal waves were disrupted by other large amplitude noise waves within the time scale of the strain readings. At that time in the testing only one bar was installed in the fixture. An example of the noise can be seen in figure 3.10. For the case shown the excitation voltage was set at 2.5 volts. The incident and reflected strain histories can be seen. By aligning the bars more precisely, using lubrication at the impact location and specimen location, and using conditioners with larger excitation voltage of 10 volts and faster frequency response of 160 kHz at -3db, the noise was able to be reduced.

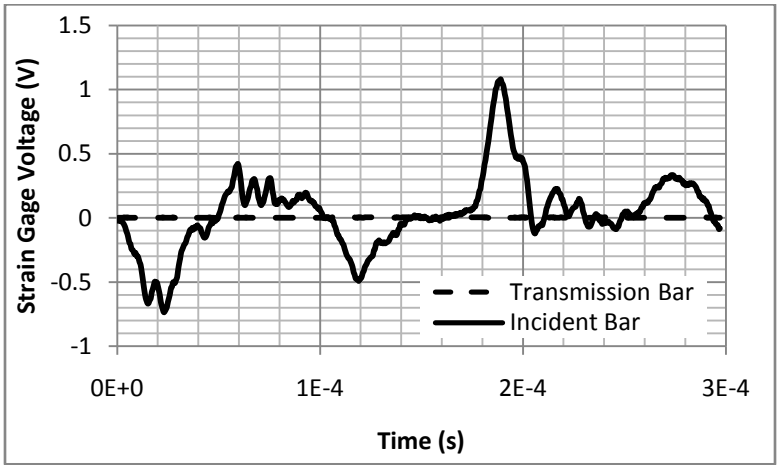

Figure 3.10 Noise Problem with Incident Bar Impacted

This noise did not seem to be related to the output signal generated by the amplifier. If the excitation voltage of the amplifier was turned off, this large amplitude noise was still observed during an impact. A graph of this noise can be seen in figure 3.11. In this case the incident bar was the only bar impacted. The transmission bar is plotted to see what the base line noise was like. The steps that were taken to solve this problem were increasing the amplifier excitation voltage to 10 volts, remounting the strain gages on the pressure bars, and installing new shielded strain gage wires. These steps reduced the impact of the noise on the strain readings.

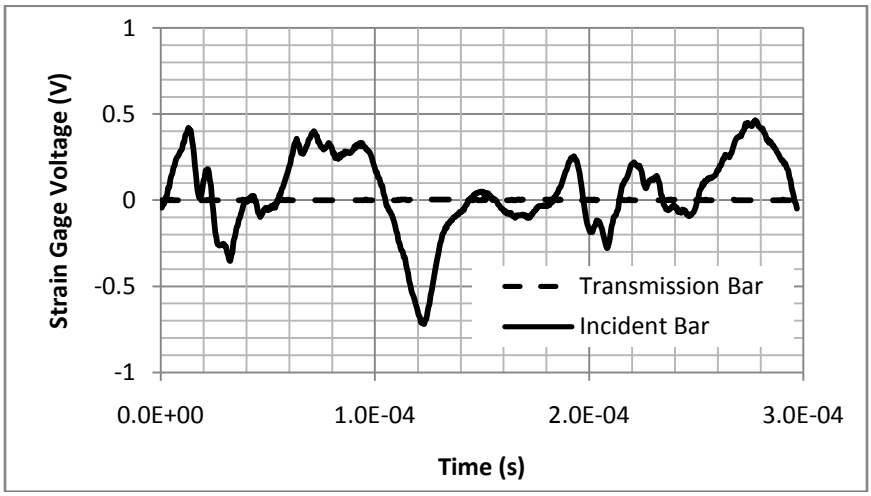

Figure 3.11 Zero Excitation Voltage Noise in Incident Bar

At one time during the investigation into this problem the voltage readings obtained from the zero excitation voltage impact could be subtracted from the 2.5 volt excitation voltage impact and a more defined curve could be observed. This was found to be impractical since the noise generated from the zero excitation impact and the noise within the 2.5 volt excitation impact was not always the same shape and amplitude. An example of the result of the subtraction is shown in figure 3.12.

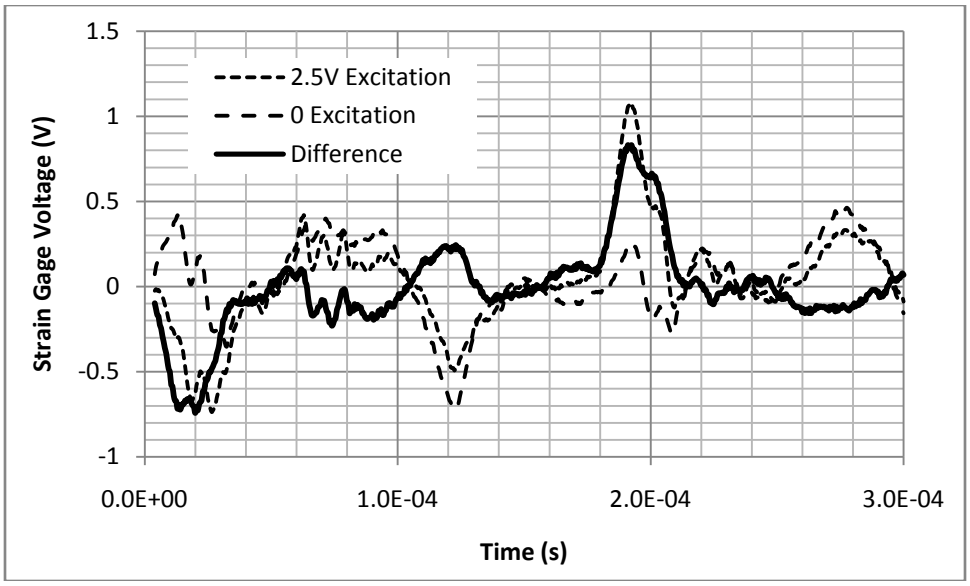

Figure 3.12 Subtraction of Excitation off and on

With further investigation to this noise problem it was determined that several things did not seem to affect this impact noise. Rotating the bar so that the strain gage was at different angles did not make a difference in the noise generated. The rotation or axial alignment was to determine if the noise generated was caused by the strain gage traveling through a magnetic field. Other areas that seemed to have little impact on the noise problem were friction of the bearings, pressure bar material, and machining the pressure bar ends square. These things did not have an observed impact although some investigators have found a lack of friction and square bar ends to be important (3).

What has seemed to work the best to reduce this noise problem was to align the bars and use only straight bars, grease the ends of the bar's at the impact location and the specimen location. To align the bars new pillow blocks were made that had adjustment screws. This reduced the noise some but not as much as was hoped. It is believed that these solutions reduce the noise problem because they help ensure linear wave

propagation in the bars. The increased excitation voltage made a large improvement on the noise reduction by increasing the amplitude of the desired strain readings.

3.3.2 Cannon Alignment

When the pressure bar was first designed, pillow blocks were machined to fit rigidly in the grooves of the Bosch tubing. This was done to ensure proper alignment since alignment is important to ensure linear wave propagation (3). Unfortunately the original bars installed were not straight and variation in machining of the pillow blocks caused a noticeable misalignment of the bars. The bore of the cannon and the bars also did not align. A majority of the original testing was done with these misaligned bars. Later the bars were replaced with straight steel bars and later with straight aluminum bars. The straightness of the bars helped some, but there was still misalignment between the bars and the cannon barrel. To fix these problem new pillow blocks were made with three setscrews spaced at 60° around the pillow block enabling the bars to be aligned with the cannon barrel.

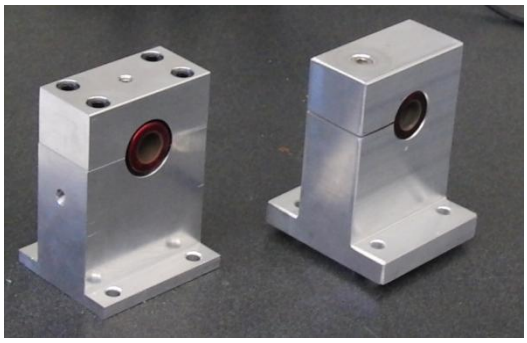

Figure 3.13 Adjustable and Rigid Pillow Blocks

Another problem that had been noticed with the cannon barrel was that the bore was machined too small. This caused the 0.5 inch striker bar to become stuck inside the

cannon when it was fired. To correct this problem the cannon barrel and the striker bars were sanded to allow smooth travel while firing. As the cannon was used there had been buildup of dirt or other debris. To fix this problem the barrel can be cleaned periodically with a rod, sandpaper and a drill. Figure 3.14 shows the setup that was used to clean the barrel.

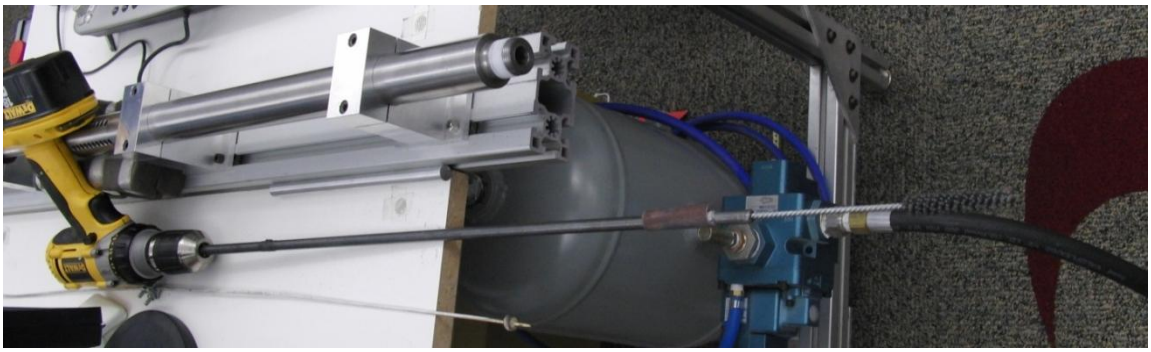

Figure 3.14 Sanding the Barrel

3.4 Summary

The design and setup of the split Hopkinson pressure bar was presented along with the operating procedure and some of the problems encountered during construction.

The split Hopkinson pressure bar was designed to test soft materials. This was done by using shorter incident and transmission bar made from aluminum. The pressure bars were instrumented with strain gages that were connected to a computer through conditioners.

To operate the pressure bar a program was written in LabVIEW. This program was used to control the firing speed by regulating the air pressure in a supply tank. Also

the LabVIEW program recorded the strain gage readings and saved those to a file for data reduction.

Some of the problems encountered while constructing and debugging the SHPB were electrical noise and cannon alignment. The electrical noise was reduced by fixing grounding issues and increasing the excitation voltage. The cannon alignment was improved by installing adjustable brackets for holding the pressure bars.

4 Experiments

4.1 Introduction

The impact properties of various softballs were tested. Softballs with different stiffness and rebound properties were compared to determine what effect stiffness and rebound properties had on their behavior. The procedures used for testing these the materials is discussed in this chapter.

4.2 Verification

To verify that the split Hopkinson pressure bar was working data obtained from the SHPB needed to be compared with data obtained from a working pressure bar. In 1973 Chou, Robertson and Rainey published an article where they tested Nylon 6/6 and other polymers using a split Hopkinson pressure bar (15). They were looking at temperature rise during testing. The sample they used was 3/8 inches in diameter and 1/2 inches in length. Using a specimen of the same size the stress strain obtained by Chou, et al. was matched quite well. The data tested in the laboratory with the SHPB was compared to that of data published by Chou in figure 4.1.

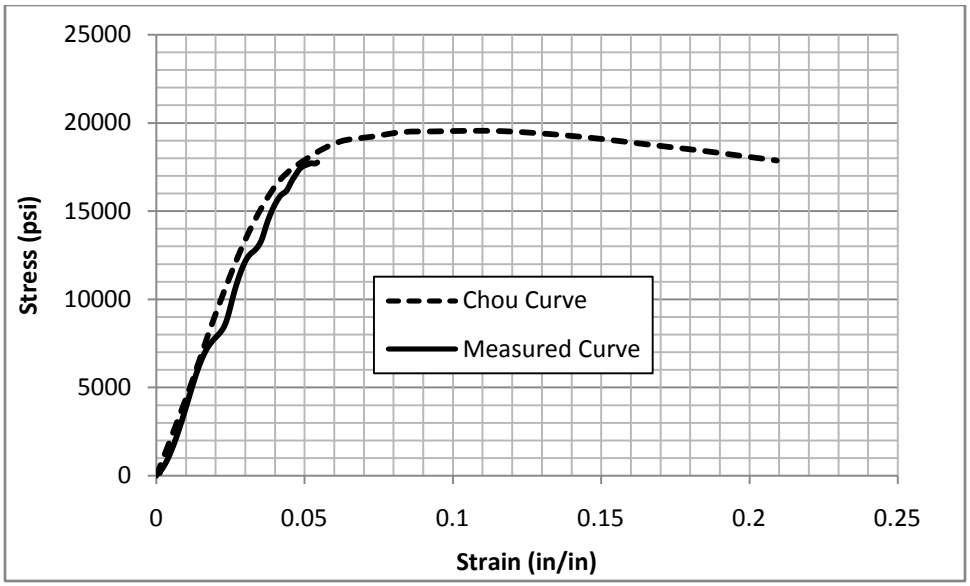

Figure 4.1 Engineering Stress and Strain of Nylon 6/6

The specimen measured in the lab was measured at an average strain rate of 644 s^{-1}. The data obtained by Chou was at a strain rate of 1250 s^{-1}. Although the strain rates are different the data agree quite well. Chou had a total engineering strain of approximately 0.2, where the data measured was at a max strain of 0.054. The reason for the difference in the strain rate and total strain was that Chou used a steel SHPB and an aluminum SHPB was used for the measured curve. Using the same specimen dimensions as Chou it was difficult to obtain the higher strain rate with aluminum bars. Because of the size of the pressure bar the total strain of 0.2 could not be reached.

The curve given my Chou was displayed in true stress and strain but was converted to engineering stress and strain. This was done so this thesis could be consistent in displaying all the data in engineering stress and strain. The data displayed in figure 4.1 is engineering stress and strain. Due to the strong correlation between the

measured values and those obtained by Chou the aluminum pressure bar data was verified.

4.3 Capabilities

4.3.1 Amplitude and Duration

There are several aspects about the split Hopkinson pressure bar that can be varied in order to test different materials. There are two factors that have a significant impact on the signal of the split Hopkinson pressure bar, the striker bar length and velocity. As the striker bar length increases the signal duration increases. This is shown below in figure 4.2. The trend of striker bar length to signal duration is linear and can be seen in figure 4.3. This shows that the signal duration is proportional to striker bar length. The striker bars used for this investigation are shown in figure 4.4.

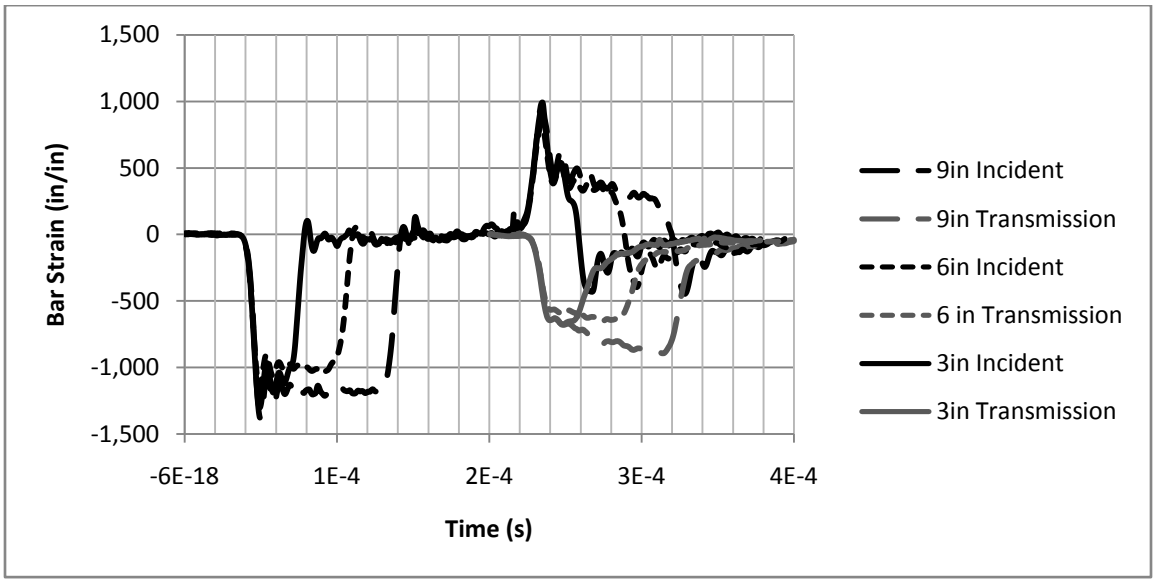

Figure 4.2 Comparison of Striker Bar Length to Signal Duration

Figure 4.3 Signal Duration Compared to Striker Bar Length

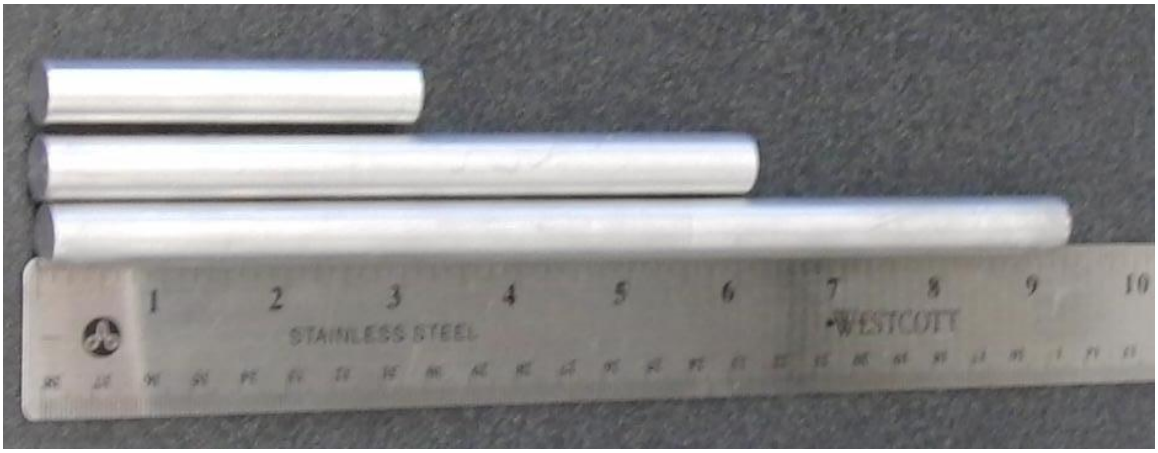

Figure 4.4 Aluminum Striker Bars

In order to attain similar amplitudes with different length striker bars the change in striker bar mass needed to be considered. Since the velocity was regulated with cannon pressure the pressure for a shorter striker bar needed to be decreased in order to match the

velocity of a longer striker bar. An equation was needed to relate the striker bar velocity to the pressure.

The velocity of the bar at the end of the cannon can be estimated using classical kinematics. If pressure is constant the energy is expressed as

$$\frac{1}{2}mv^2 = PA(L - L_c), \qquad 4.1$$

where m is the bar mass, v is the bar velocity, P is the pressure, A is the bar cross-sectional area, L is the cannon length, and L_c is the length of the striker bar. It follows that the calculated velocity at the end of the barrel can be expressed as

$$v = \sqrt{PA\frac{2(Lc - L)}{m}}. \qquad 4.2$$

This equation is neglecting the frictional effects in the cannon.

Although this equation is an estimate and does not account for friction, it can be used for comparisons between bar lengths to attain similar velocities. The pressure can be taken as the measured tank pressure. The pressure in the cannon is unknown, but should be less than the accumulator pressure and the cannon pressure should be constant. Equation 4.2 was used to achieve similar amplitudes in figure 4.5.

The signal is also affected by the velocity of the striker bar. As the striker bar's velocity increases the signal amplitude increases. This can be seen in figure 4.5. To increase the amplitude the cannon pressure was increased which increases the striker bar velocity. The average bar strain is compared to the accumulator pressure in figure 4.6. Although amplitude does not increase linearly with pressure there is a noticeable trend.

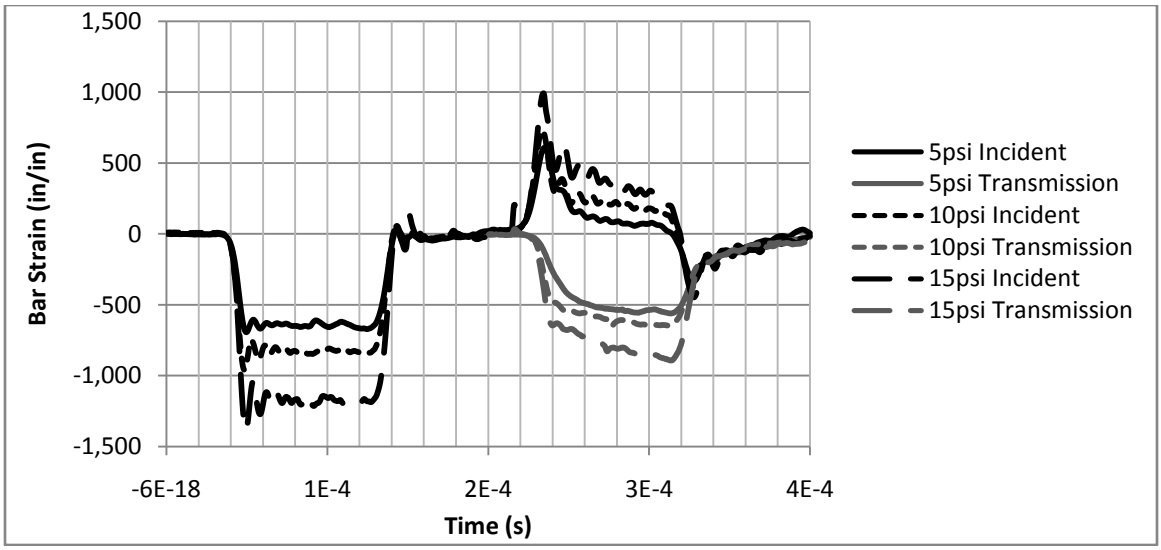

Figure 4.5 Comparison of Striker Bar Velocity Using a Striker Bar Length of 9 in

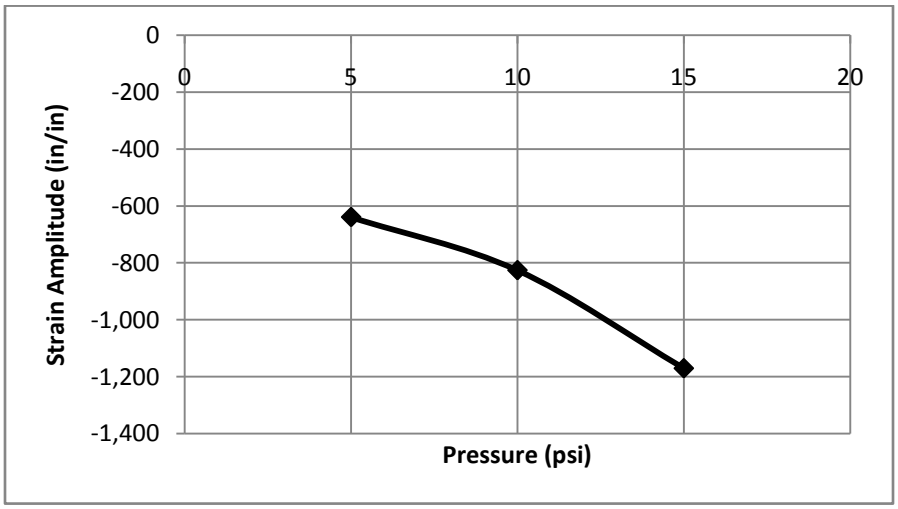

Figure 4.6 Strain Amplitude Compared to Accumulator Pressure

The general trends associated with the change in striker bar length and velocities were as expected. The increased amplitude due to increased striker bar velocity and increased duration due to increased striker bar length were discussed by Gray (3).

4.3.2 Shaping

Changing the shape of the incident wave changes the way the specimen is loaded and can help in attaining uniform stress distribution. There are several techniques that can be used to change the shape of the incident wave. One technique is to change the shape of the striker bar. Another technique is to place something between the striker bar and incident bar (10; 19). An example of a wave history where shaping has been used is shown in figure 4.7.

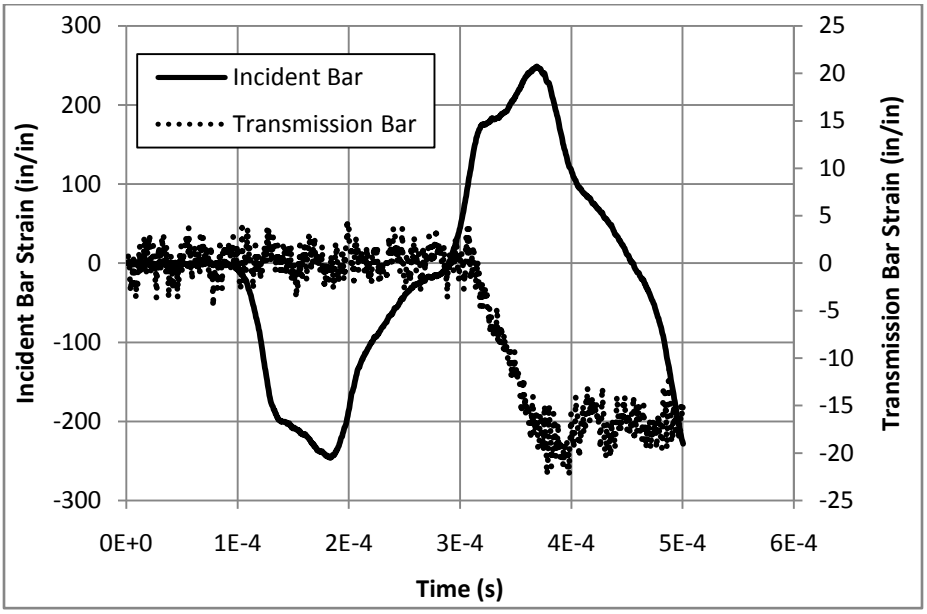

Figure 4.7 Strain History in Pressure Bars with Shaping Used

To shape the waves tips were made for the striker bar. These tips were designed to sit in front of the striker bar and change the shape of the loading side of the incident strain wave. It was found that the gap between the striker bar and tip created excess noise and made the data difficult to reduce. Figure 4.8 shows some of the different tips that were used to shape the waves. Wave shaping using shaping tips was not used for the testing of

polyurethane due to the increased noise from shaping techniques caused by the alignment as well as the joint between the shaping tip and striker bar.

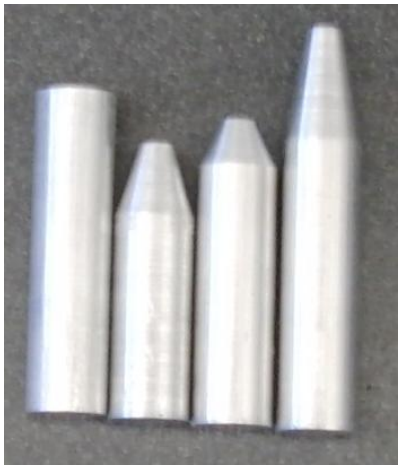

Figure 4.8 Incident Shaping Tips

The other technique for shaping the incident wave was the use of inserts between the striker bar and incident bar. Copper was looked at for shaping. Different sizes of inserts were applied for wave shaping. With copper it was found that the inserts also created an increase in the signal noise.

It was determined that the signals that were being generated from the cylindrical striker bar were sufficient for the characterization of polyurethane. Because of this, further work in wave shaping was not conducted.

4.3.3 Polyurethane Specimen Size Effects

The specimen size was selected based on several factors. The signal transmission and construction were the main factors. There were some investigative experiments

conducted to determine what length would enable signal transmission. The tools available for specimen construction were also a factor.

At first a larger sample size was investigated. The size was 0.25 inches in diameter and 0.25 inches in length. A picture of the sample is shown in figure 4.9. It was found that the transmitted signal was too small to distinguish between the signal and the line noise.

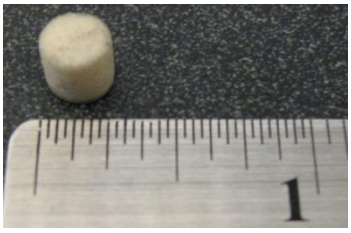

Figure 4.9 First Polyurethane SHPB Test Sample

This first sample was created on a lathe. The polyurethane foam was turned down to 0.25 inches in diameter and then cut into 0.25 inch lengths. Thinner samples were needed in order to increase the signal to noise ratio. A new technique was needed for the thinner samples because it was too difficult to cut lengths less than 0.25 inches and have the faces parallel.

To attain thinner specimens the softball was cut into thin sections on a band saw and sanded flat. These thin sections, example shown in figure 4.10, could then be cut into circles and used as test specimens. The diameter of the specimen was determined by the punch size available. When these thinner specimens were tested a larger transmitted signal was observed.

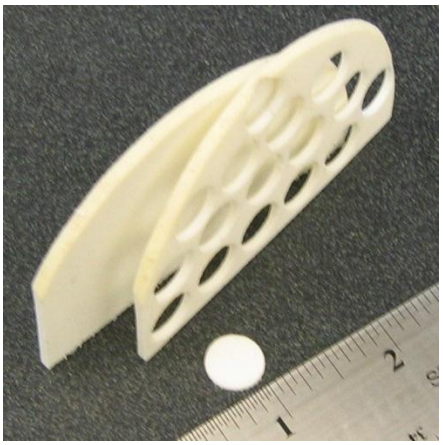

Figure 4.10 Thin Specimen Construction

4.4 Polyurethane Introduction

4.4.1 Introduction

Softballs of different stiffness and rebound properties were compared in various test throughout this thesis. There were five different models of softballs tested. Refer to table 4.1 for a list of the models and advertized nominal properties COR and compression.

Table 4.1 Ball COR and Compression

Manufacture	Ball Code	COR	Compression (lbs)
Dudley	WT11 ND Y-1	.44	525
Diamond	12RSC 44	.44	300
Worth	SX44RLA3	.44	375
Diamond	12RFPSC 47	.47	375
Diamond	12RSC 40	.40	375

Softballs with different COR values were selected. To reduce the number of variables balls with the same nominal compression were selected. This will help determine how the COR effect different properties.

Another aspect about the softballs that was investigated was the stiffness. Softballs with different stiffness properties having the same COR were selected. The softballs were compared using dynamic stiffness (DS) but were selected based on their compression values.

There is variation in the manufacturing process. A manufacture may advertise a ball as .44 COR and 375 compression but the actual values of COR and compression are usually different. Each ball that was tested was purchased in a lot of one dozen balls. Two of each ball model were cut up for test specimens and six balls from each model were tested to determine the lots average COR and compression. The average COR and compression for each ball model are shown in table 4.2.

Table 4.2 Measured Average Ball Properties with Standard Deviation in Parenthesis

Manufacturer	Model	Nominal COR/Comp	COR Average	Comp Average lbs	DS Average lbs/in
Dudley	WT11 ND Y-1	.44/525	0.454 (0.006)	652 (8)	12259 (450)
Diamond	12RSC 44	.44/300	0.425 (0.004)	247 (4)	5424 (170)
Worth	SX44RLA3	.44/375	0.442 (0.004)	360 (14)	6744 (160)
Diamond	12RFPSC 47	.47/375	0.462 (0.005)	338 (8)	5570 (170)
Diamond	12RSC 40	.40/375	0.426 (0.004)	440 (6)	5606 (170)

Upon examination of the average ball properties in table 4.2 it is evident that the actual ball properties differ from the nominal values. Some ball models are closer to the nominal values than others.

Other investigators have looked at testing polyurethane with a spit Hopkinson pressure bar (4). They found that the properties of the polyurethane foam were dependent on density. For a better comparison to this research the density has been calculated for each ball by measuring the circumference and weight and calculating the density. These results are shown in table 4.3.

Table 4.3 Ball Density

Manufacture	Ball Code	COR	Comp lbs	Density oz/in^3 (kg/m^3)
Dudley	WT11 ND Y-1	.44	525	.267 (462)
Diamond	12RSC 44	.44	300	.212 (367)
Worth	SX44RLA3	.44	375	.211 (365)
Diamond	12RFPSC 47	.47	375	.208 (361)
Diamond	12RSC 40	.40	375	.204 (354)

4.4.2 Polyurethane Cell Comparison

Each ball has a slightly different density and different rebound and stiffness properties. To understand how the cell structure affects these properties each ball was looked at under a microscope. Pictures of each ball under M10 magnification are shown below in figure 4.11. The view is about 1/32 by 1/32 inches.

The light circles in these pictures are foam cells that are open. It appears that the cell size changes between ball models. Looking at specimens 12RSC 40 (40/375), SX44RLA3 (44/375), and 12RFPSC 47 (47/375) it looks like the cell size increases as

COR increases. Comparing 12RSC44 (44/300), WT11NDY-1 (44/525), and SX44RLA3 (44/375) it looks like the compression also increase as cell size increases.

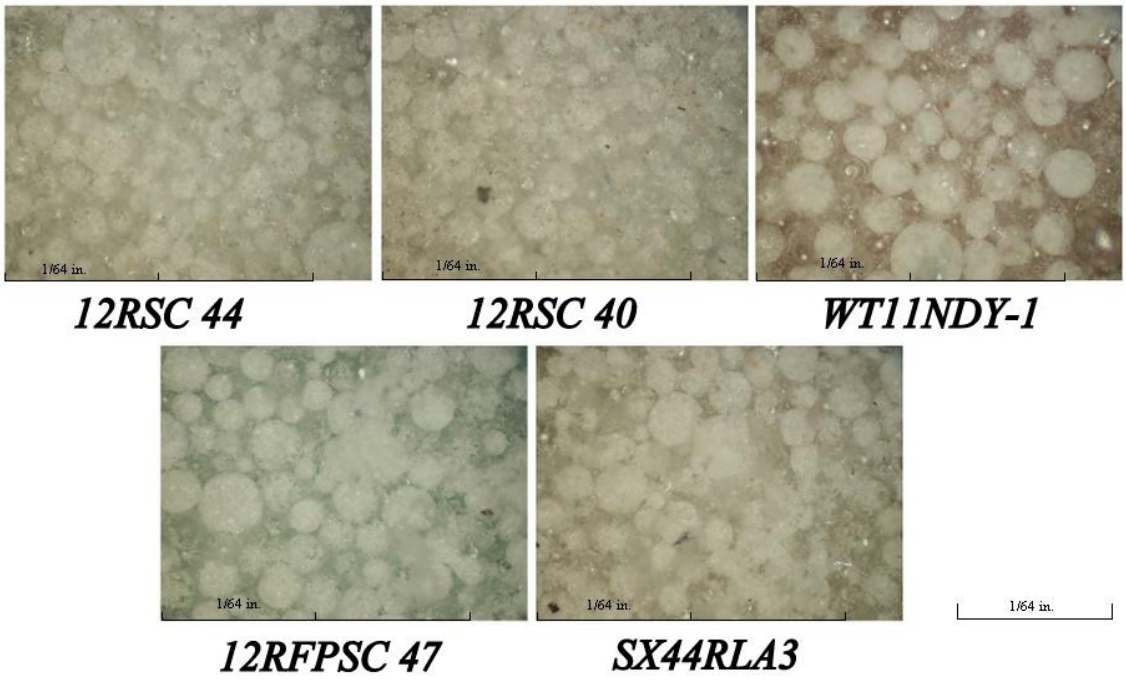

Figure 4.11 Magnified M10 Cross-Section of Ball Specimens

4.4.3 Finite Element Model

When the softball is impacted with the bat, the ball can experience strain at very large strain rates. To model the bat-ball interaction, the properties of the softball at high strain rates are needed. Using existing models the highest strain rate that is seen in the ball is about 2500 s^{-1}. Figure 4.12 shows the strain rate as a function of time predicted by a finite element model. The strain is 0.074 in/in at the peak strain rate.

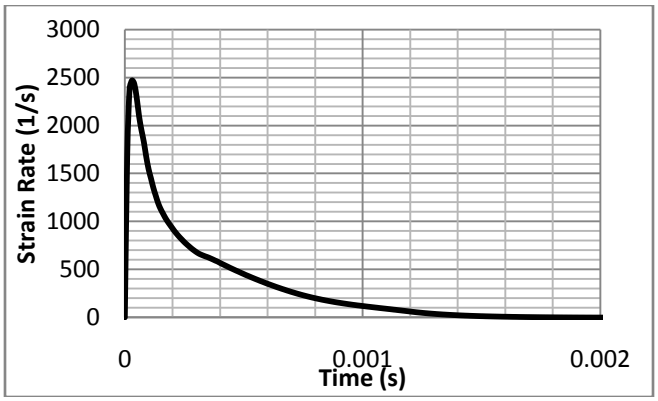

Figure 4.12 Strain Rate in Ball Collision

Based on initial investigations the duration of the strain in the split Hopkinson pressure bar test is 8.0E-5. This was based on tests using a nine inch striker bar. Figure 4.13 shows the same data as seen in figure 4.12 but with an adjusted time scale to match what is seen in a SHPB test. Based on the data obtained from the initial finite elements test the goal for the split Hopkinson pressure bar test was to obtain strain rates similar to those seen in figure 4.13.

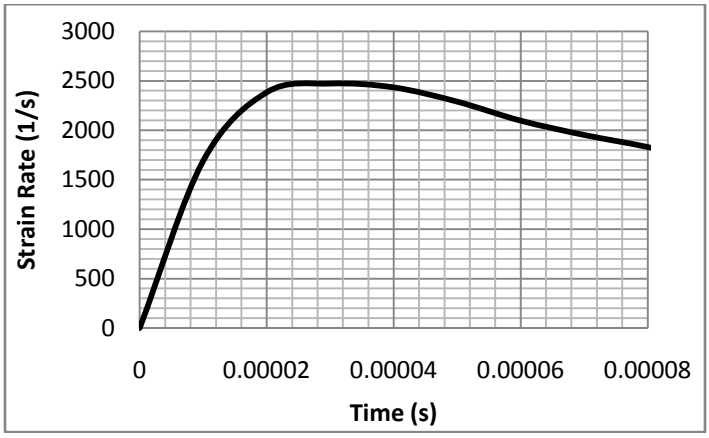

Figure 4.13 Strain Rate in Ball Collision Short Time Scale

The finite elements model used to calculate figure 4.12 and figure 4.13 was created in LS-DYNA. These models are part of Warren Faber's research (2). In figure

4.15 the mesh used to model the bat ball impact is shown. The lower mesh that is circled is the mesh that was used to display the strain rate in figure 4.13. On the left side is the mesh before the impact and on the right the mesh is during the impact in the deformed state.

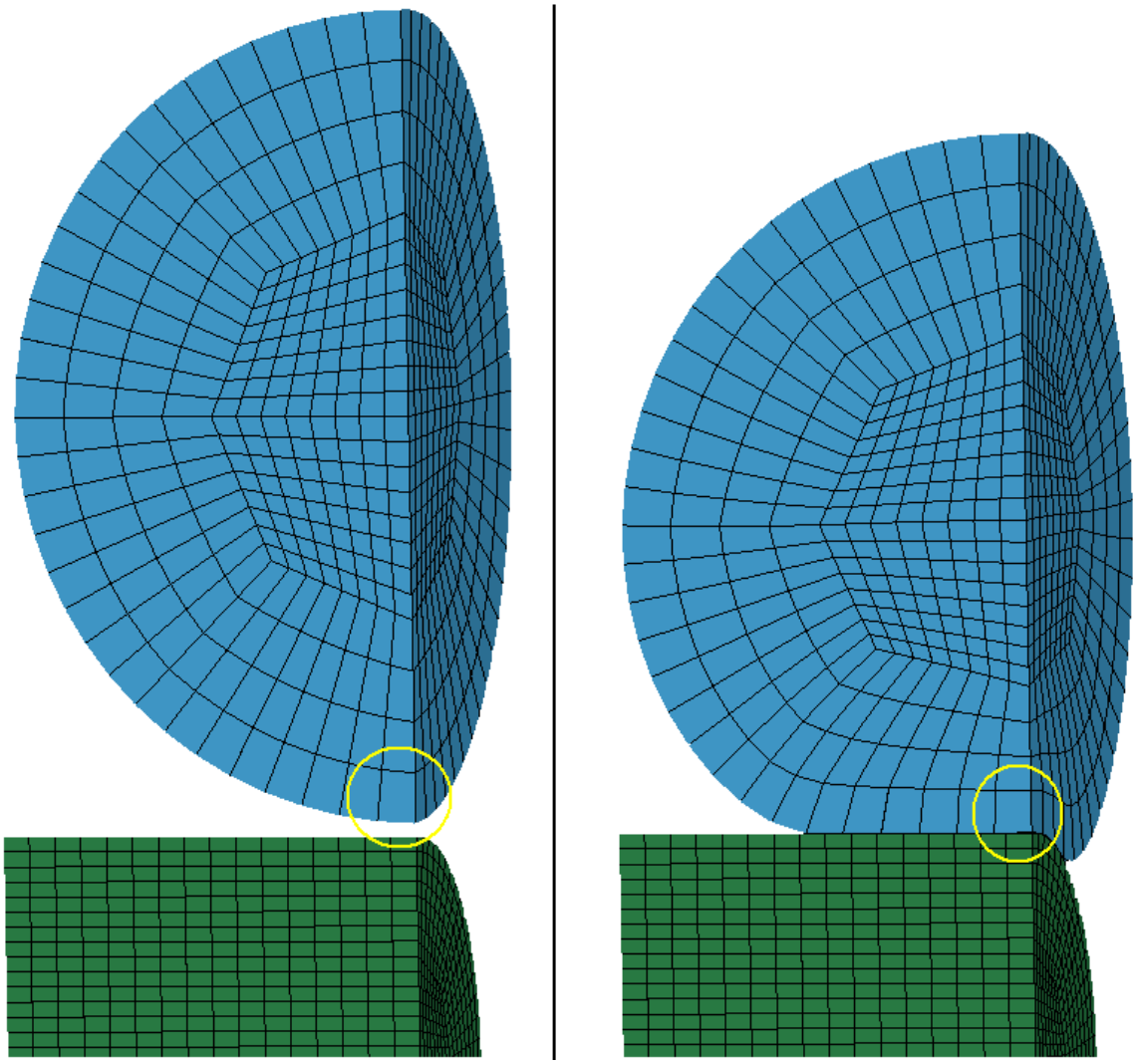

Figure 4.14 Finite Element Ball and Bat Mesh, Before Impact (left), During Impact (right)

4.4.4 Viscoelastic Response

Polyurethane is a viscoelastic material meaning the strain is time dependent and stress dependent. Because the strain is dependent on time a viscoelastic model was used to model the behavior of the polyurethane material. This viscoelastic model was also used in the FEA model of the ball. Below is the development of the viscoelastic stress strain equation.

The classical response of a linear viscoelastic material from a strain input is described by

$$\sigma(t) = \int_0^t E(t-\tau)\dot{\varepsilon}(\tau)d\tau \quad , \qquad 4.3$$

where E is the relaxation modulus (20). The relation between the elastic modulus and the shear modulus is shown as

$$E = 2G(1-\nu) \quad , \qquad 4.4$$

where E is the elastic modulus, G is the shear modulus and ν is the poisons ratio.
The time dependent shear modulus using the numeric model is given by

$$G(t) = G_\infty + (G_o + G_\infty)e^{-\beta t} \quad . \qquad 4.5$$

Combining equation 4.4 with equation 4.5 the elastic modulus can be expressed in terms of the shear modulus as

$$E(t) = 2(1+\nu)(G_\infty + (G_0 + G_\infty)e^{-\beta t}) \quad . \qquad 4.6$$

The strain that is seen by the specimen is applied at a constant rate R and is zero until time t

$$\varepsilon(t) = RtH(t), \tag{4.7}$$

where the step function H(t) is defined as 0 for t < 0 and 1 for t > 0. Taking the time derivative of equation 4.7 gives

$$\dot{\varepsilon}(t) = RH(t) + Rt\delta(t) \tag{4.8}$$

which is the strain rate. The function δ(t) is the derivative of the step function H(t) and is zero everywhere except at t = 0 where it is 1.

Substituting equations 4.6 and 4.8 into equation 4.3 the stress can be expressed in terms of the viscoelastic parameters G_∞, G_o, and β as

$$\sigma(t) = \int_0^t 2(1+\nu)(G_\infty + (G_o + G_\infty)e^{-\beta(t-\tau)})(RH(t) + Rt\delta(t))d\tau, \tag{4.9}$$

where the terms *v* and *R* are constants.

Since positive time is the only time of interest the step function H(t) is one for all time being considered. Also the tδ(t) term is always zero since δ(t) is nonzero only when t equals zero. Moving the constants out of the integral and applying the known values for the delta function and the step function yields

$$\sigma(t) = 2R(1+\nu)\int_0^t (G_\infty + (G_o - G_\infty)e^{-\beta(t-\tau)})d\tau. \tag{4.10}$$

Taking the integral then yields the stress in terms of known constants

$$\sigma(t) = 2R(1+\nu)\left(G_\infty t + \frac{G_o - G_\infty}{\beta}(1 - e^{-\beta t})\right). \tag{4.11}$$

Equations 4.7 and 4.11 can be used to calculate the stress strain behavior of a viscoelastic material. For polyurethane the parameters used to calculate the viscoelastic stress strain response in the numeric model are shown in table 4.4. Using the parameters in table 4.4 the stress strain curves were plotted in figure 4.15.

Table 4.4 Polyurethane Parameters for Viscoelastic Model

Properties	Values			
Dynamic Stiffness (lb/in)	4689	6227	9857	11339
Density (lb/in^3)	3.975E-05	3.975E-05	3.975E-05	3.975E-05
G_o (psi)	15000	20000	30000	35000
G∞ (psi)	680	1000	1800	2200
β (s^{-1})	68000	68000	68000	68000
R (s^{-1})	2500	2500	2500	2500

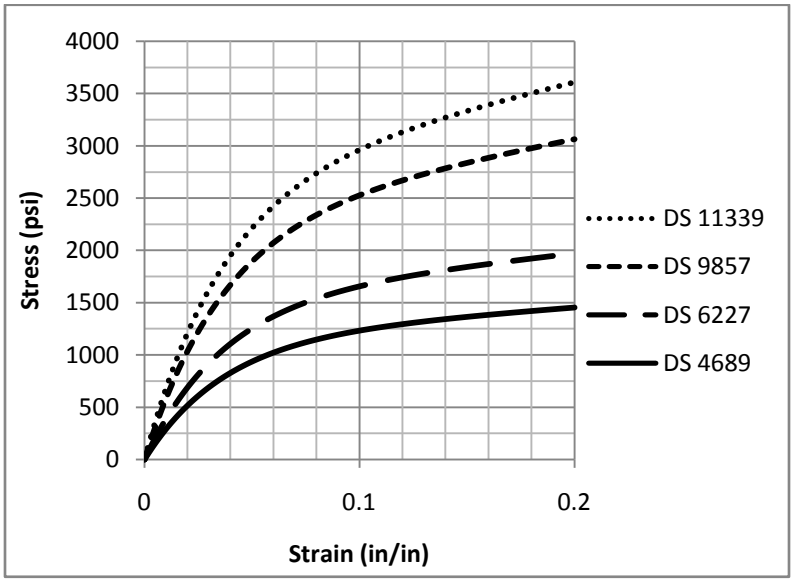

Figure 4.15 Predicted Viscoelastic behavior of Polyurethane

As the dynamic stiffness decreases the amplitude of the numeric stress strain curve also decreases as seen in figure 4.15. This predicted curve will be compared to the data collected in the discussion section of this chapter.

4.5 Low strain Rate Testing

4.5.1 Low Strain Rate Test

For comparison with the high strain rate testing done with the SHPB, low strain rate tests were conducted to compare the properties of the softballs. An MTS load frame was used to measure the load and displacement of the samples. The setup used is shown in figure 4.16. The sample was placed between two flat plates and compressed. Figure 4.17 shows the compressed state of the sample.

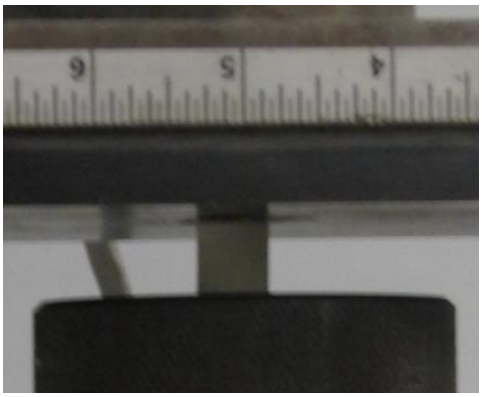

Figure 4.16 Low Strain Rate Compression Setup

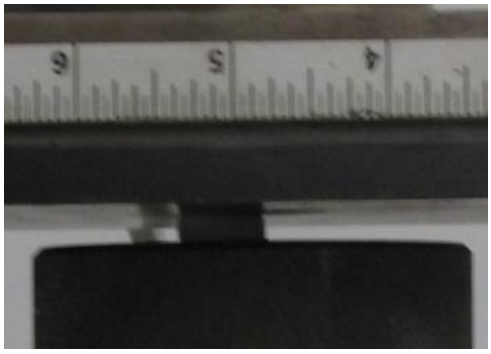

Figure 4.17 Low Strain Rate Compressed Sample

The nominal dimensions of the sample cylinders that were compressed were 0.5 inches in diameter and 0.53 inches in length. The samples were made by cutting the softball into long one inch square blocks using a band-saw. These long blocks were then mounted into a lathe and turned down to 0.5 inches. The long cylinders were then cut to length on a ban-saw. The ends were sanded flat to give a good surface to contact. The ends of the sample were greased before placing them in the load frame. The samples were compressed at a constant rate of 10 inches per second which gives a strain rate of 0.33 s^{-1}. The displacement and load were read and recorded from the load frame using an attached computer.

4.5.2 Stress Strain Results

From load-displacement data the engineering stress and strain were calculated and plotted in figure 4.18 and figure 4.19. Figure 4.18 shows the stress strain curves for the varied DS samples and figure 4.19 shows the stress strain curves for the varied COR samples.

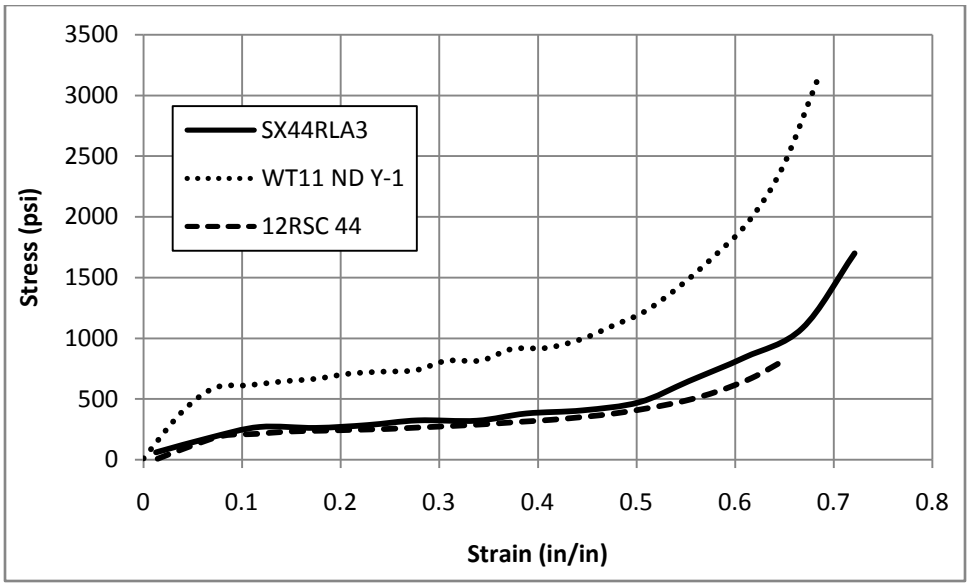

Figure 4.18 Varied DS at 0.33 s^{-1} Strain Rate

The general shape of the stress-strain curve is typical of rigid foams. This was discussed in section 2.5.3. There is an initial section where the polyurethane foam behaves rather linear, then after about 0.08 strain, the slope levels out. The last section the slope increases again. In the first section the foam is withstanding the load placed on it. After this point the cell walls began to buckle giving the flat region. The increased amplitude at the end is because the cells have compressed and collapsed and the slope is more a measure of the polyurethane material rather than the foam (4).

It is expected that the DS will have a noticeable impact on the stress-strain behavior. The changes in behavior of different DS balls are expended to be proportional to the measured DS.

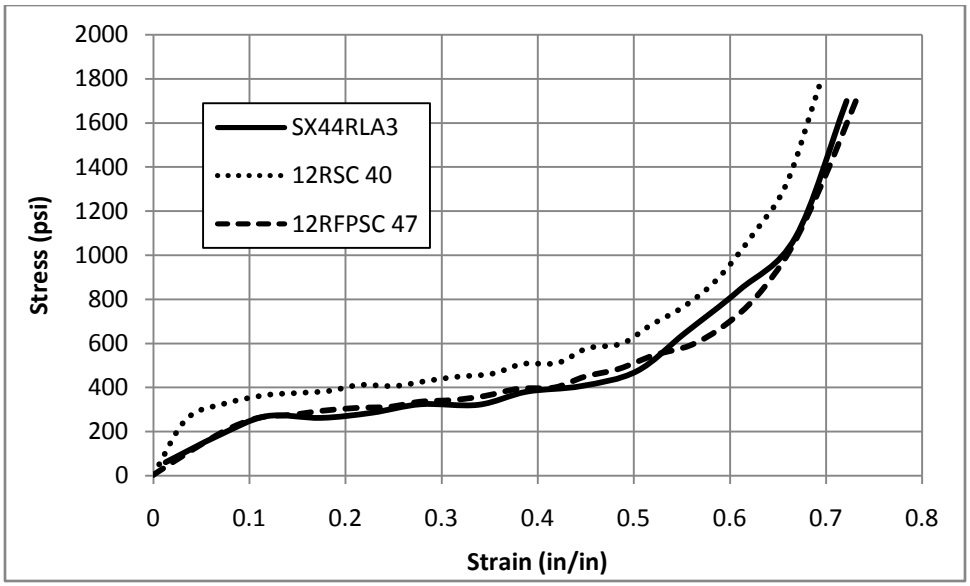

Figure 4.19 Varied COR at 0.33 s^{-1} Strain Rate

In the varied COR graph it is expected that COR would not have a large effect on the stress-strain behavior. This is because COR is a measure of the rebound properties not of the materials stress-strain behavior. Upon examination of figure 4.19 it can be seen that the curves are very similar. Refer to table 4.2 for the measured properties of these balls. The difference between the curves in the varied COR graph can be attributed to the variation in the DS not the variation in the COR. It is expected that for balls having the same DS these curves would be the same.

4.5.3 Modulus

The modulus was found for the low strain rate stress-strain curves in figure 4.18 and figure 4.19. There are several sections in the stress-strain curve of the polyurethane core. Each section has its own modulus. The modus that was calculated is for the initial rise section that is linear. This linear section ends at a strain around 0.08. The modulus

values are shown in table 4.5. The measured COR and DS for each ball are also displayed.

Table 4.5 Ball Modulus of Elasticity at 0.33s^{-1} Strain Rate

Manufacturer	Model	Nominal COR/Comp	COR Average	DS Average (lbs/in)	Low Strain Rate Modulus (psi)
Dudley	WT11 ND Y-1	.44/525	0.45	12259	7788
Diamond	12RSC 44	.44/300	0.42	5424	3041
Worth	SX44RLA3	.44/375	0.44	6744	3637
Diamond	12RFPSC 47	.47/375	0.46	5570	2948
Diamond	12RSC 40	.40/375	0.43	5606	4101

There is a trend in the modulus associated with DS. This can be seen in figure 4.20. The modulus increased as the DS increased as expected.

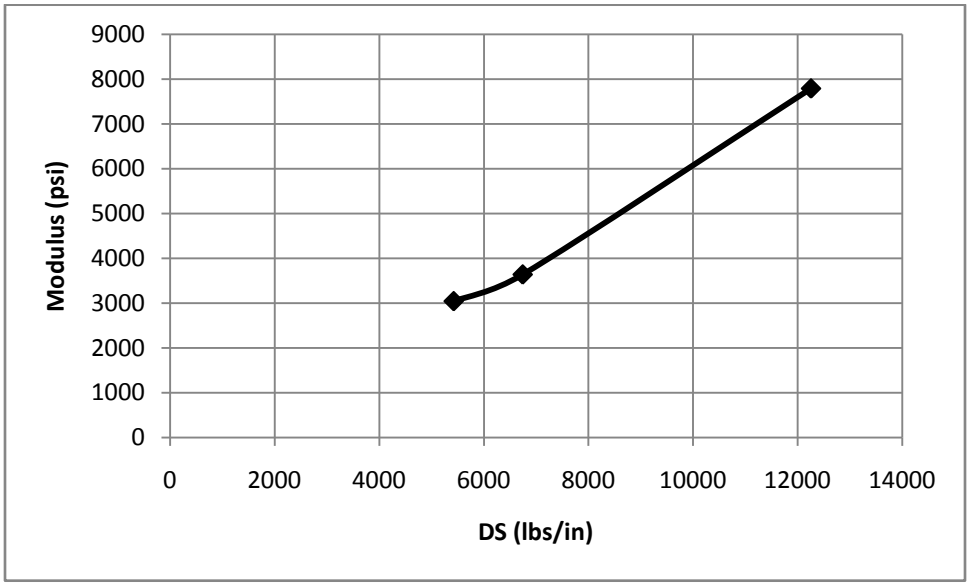

Figure 4.20 Low Strain Rate Modulus Compared with DS for .44 COR Balls

The modulus decreases with increased COR values, shown in figure 4.21. The increase in modulus due to COR may not be dependent on COR but dependent on the change in the DS average.

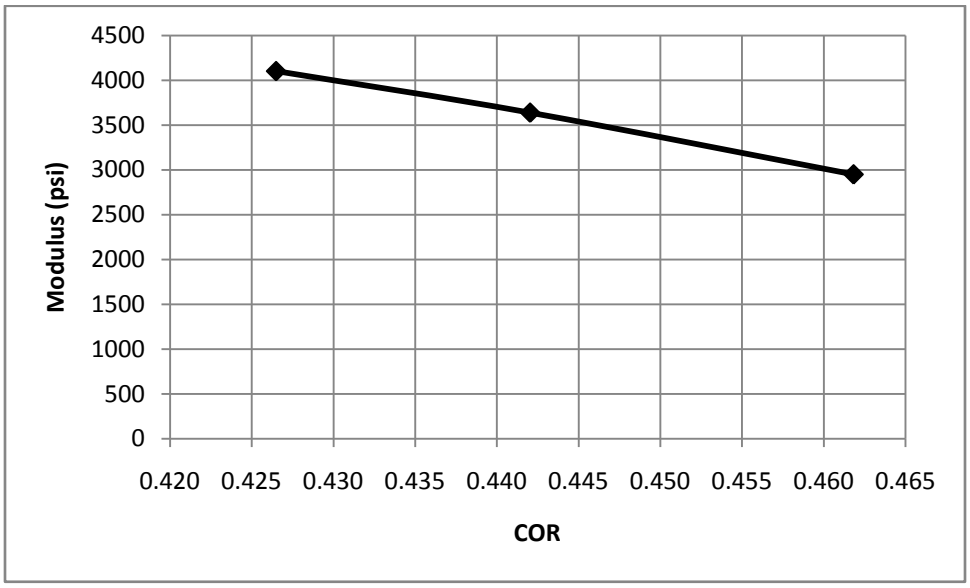

Figure 4.21 Low Strain Rate Modulus Compared with Measured COR for 375 Compression Balls

4.5.4 Hysteresis

Another aspect of the softballs that was measured at low strain rates was the hysteresis curve. This experiment was also done using the MTS universal testing machine. The strain curves are shown in figure 4.22 and figure 4.23. The specimens were loaded until they reached approximately 0.2 strain, then they were released at the same rate they were loaded. The ramp rate for the testing machine was set at 1 in/min. The nominal length of the specimens was 0.5 inches. The strain rate was 0.03 s^{-1}, this strain

rate was used so the compression could be stopped at desired deformations and to allow recovery.

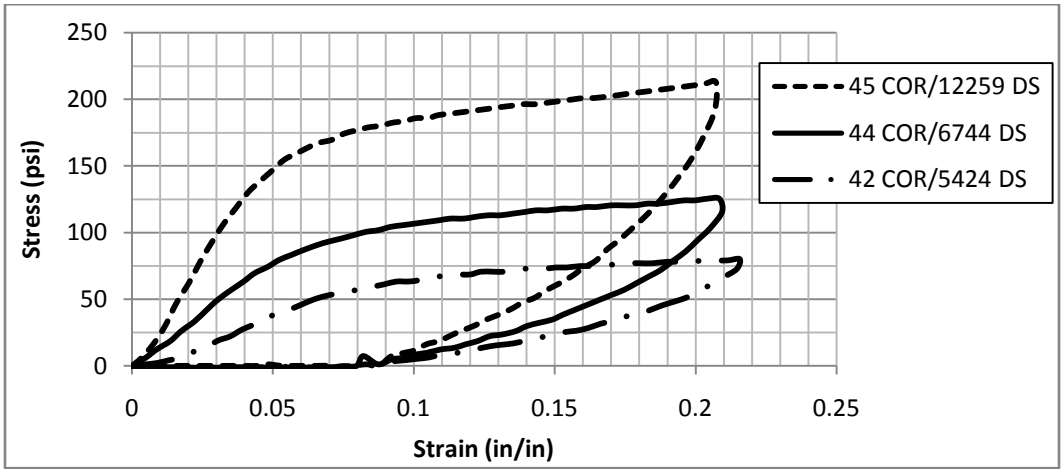

Figure 4.22 Hysteresis Comparison with Varied Stiffness

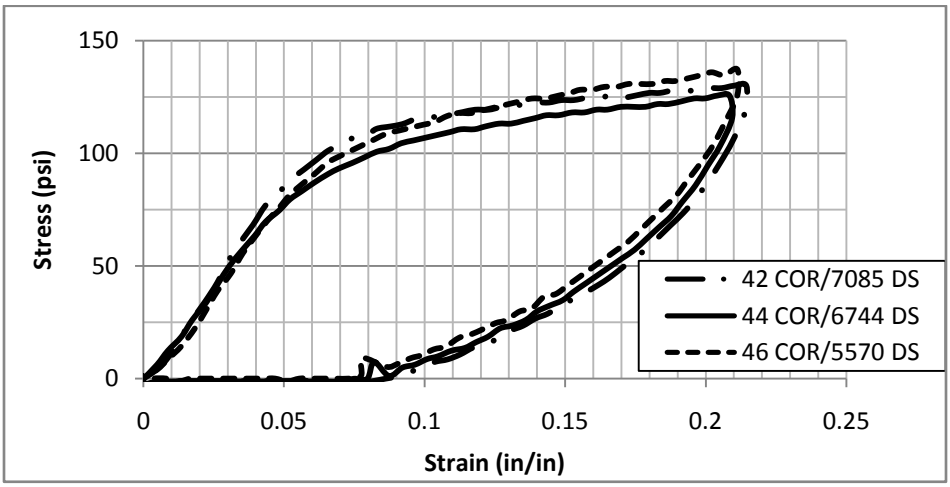

Figure 4.23 Hysteresis Comparison with Varied COR

The COR is a measure of the amount of energy retained in a system after a collision. The hysteresis of softballs with the same COR should be the same. Softballs of different stiffness traveling at the same velocity will have different displacements and strains. The hysteresis displayed in figure 4.22 and figure 4.23 where loaded to the same

deformation. To compare balls with different stiffness the deformation should decrease with increasing ball stiffness.

Using the energy of the ball

$$E = \frac{1}{2}kx^2, \qquad 4.12$$

where k is the DS and x is the deformation, the energy can be matched for each ball. DS is the stiffness of the softball and this is different from the stiffness of the specimen tested. Since the specimens tested are the same size the correlation between DS and the stiffness is assumed to be the same for the softballs being compared. Once a desired energy is selected the deformation can be calculated. This was done for the balls with different DS and the result is shown in figure 4.24.

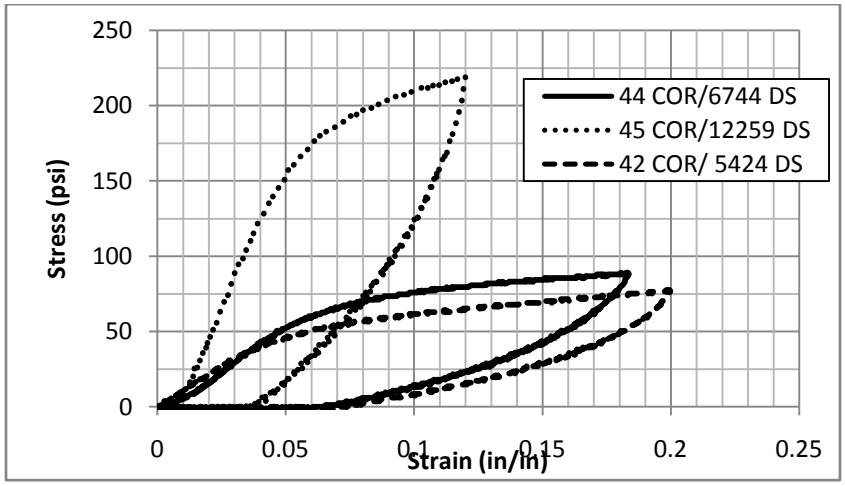

Figure 4.24 Constant Energy Hysteresis for Varied DS

Since there was some difference in the DS of the group of balls having different COR, they were also loaded to displacements as a function of ball stiffness. These tests

were also measured using different deformations. The results for varied COR softballs are shown in figure 4.25.

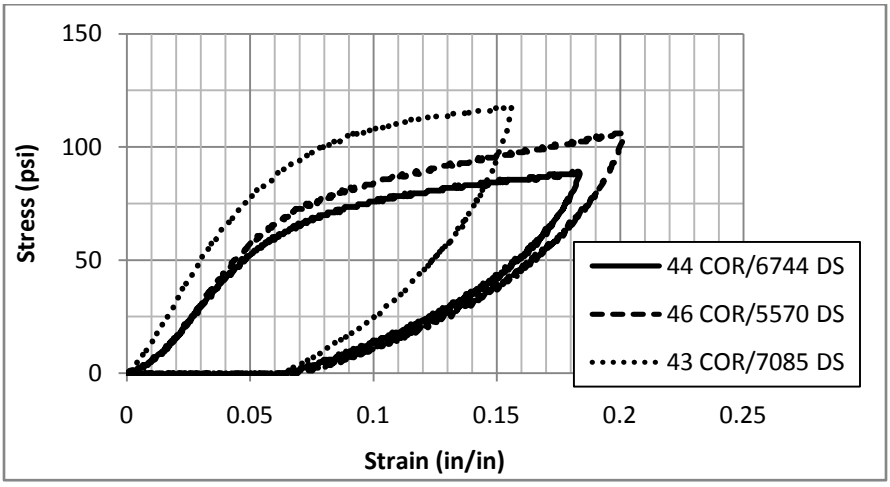

Figure 4.25 Constant Energy Hysteresis for Varied COR

The strain energy density of the curves shown in figure 4.24 and figure 4.25 was calculated. The values are shown in table 4.6. The strain energy density for the varied COR and stiffness are shown in figure 4.27 and figure 4.26.

Table 4.6 Strain Energy Density of Softballs at Constant Energy

Manufacture	Ball Code	COR	DS (lbs/in)	Strain Energy Density (psi)
Dudley	WT11 ND Y-1	0.45	12259	10.3
Diamond	12RSC 44	0.42	5424	7.7
Worth	SX44RLA3	0.44	6744	7.8
Diamond	12RFPSC 47	0.46	5570	9.9
Diamond	12RSC 40	0.43	5606	9.6

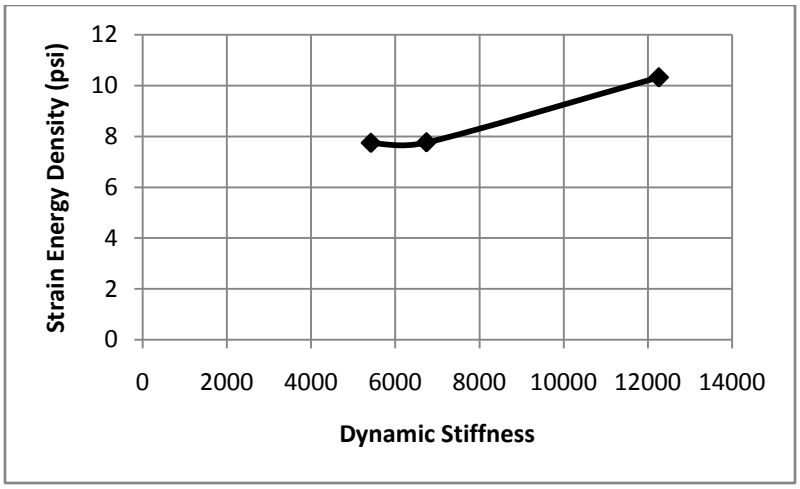

Figure 4.26 Strain Energy Density as a Function of DS for Varied DS Softballs

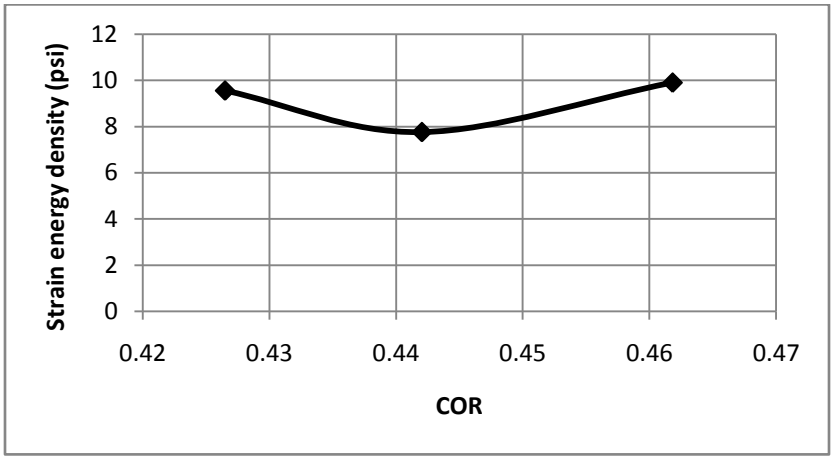

Figure 4.27 Strain Energy Density as a Function of COR for Varied COR Softballs

With the adjustment for constant energy the strain energy density is not constant for different DS balls. With varied COR softballs it was expected that the strain energy density would increase with increased COR. This was not observed in the results. There could be several reasons for this. First the deformation that was predicted for constant energy could be off due to the use of DS for the stiffness. The average DS may be different from the DS of the particular ball tested. Another reason the results were not as

expected could be that the COR is tested at impact which takes place at high strain rates. The tests were conducted at low strain rates. The strain rate sensitivity of the balls is probably the primary factor.

4.6 High strain Rate Testing

4.6.1 Specimen Construction

Because of the problems discussed in section 2.4.2 dealing with the testing of soft materials, the test specimen needed to be thin. This was to ensure the specimen attained uniform stress distribution more quickly. To make the specimens a thin slice of the softball was cut using a band-saw. The tools used to construct the specimens are shown in figure 4.28. A close up picture of the test specimen is shown in figure 4.29. The average thickness of the test specimens was 0.08 inches. Once the section had been cut from the softball the surface was cleaned with compressed air then sanded smooth. Using a hole punch the specimens were stamped out of the softball section. The diameter of the specimens was 0.44 inches.

Figure 4.28 Specimen Construction and Tools

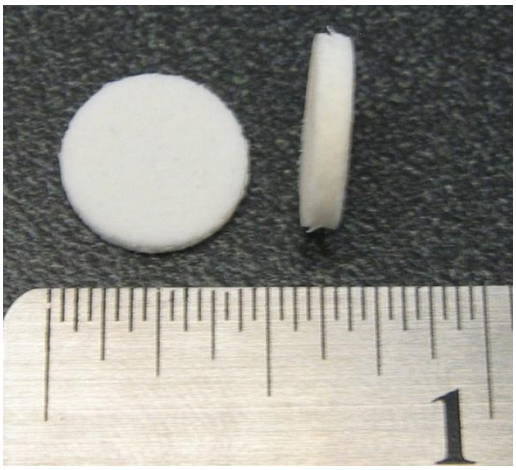

Figure 4.29 High Strain Rate Test Specimen

4.6.2 Stress and Strain at High Strain Rates

Polyurethane is sensitive to temperature and humidity. Because of this the high strain rate tests were done in an environment where the temperature and humidity were constant and controlled. The temperature and humidity during the test were 72°F and 50% RH. There were many specimens made from each ball. Each specimen was only tested once. The specimens were made from new balls so that the effects of wear from impacts due to ball testing were not present.

The high strain rate tests were done using a SHPB with aluminum bars. The pressure used for firing was 5 psi. The striker bar length was 9 inches. The excitation voltage of the signal conditioners were 10 volts. An example strain reading from the strain gages during a test is shown in figure 4.30. The incident and reflected curves are quite large and the transmission curve is very small. Because the signal is so small there is more variation due to signal noise.

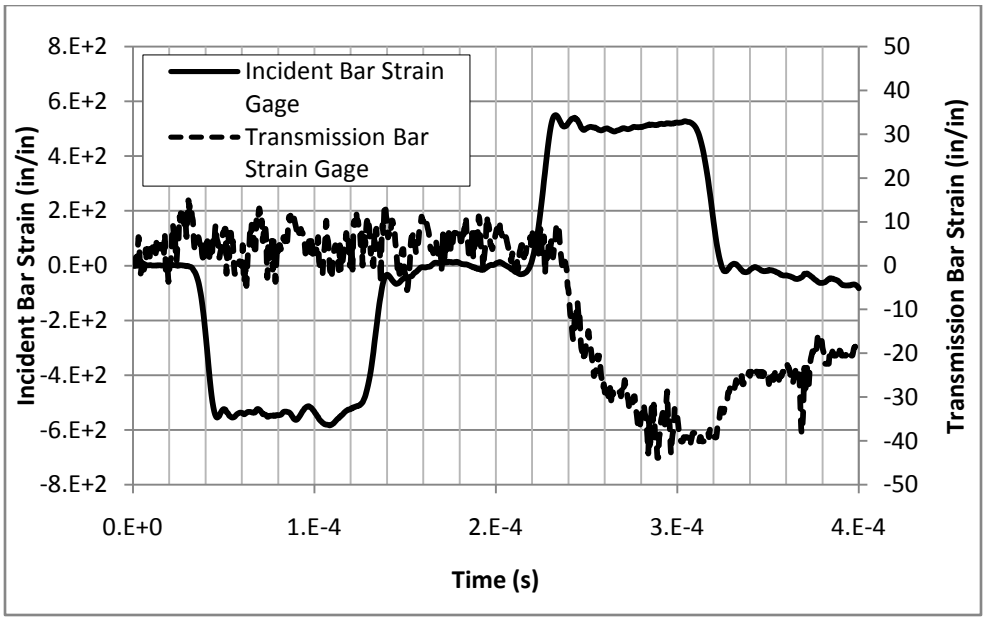

Figure 4.30 Example Strain Gage Readings for Polyurethane

The data was reduced using the equations in section 2.2.3, repeated here

$$\dot{\varepsilon} = \frac{2C_o}{L}\varepsilon_R, \qquad 4.\ 13$$

$$\varepsilon = \frac{2C_o}{L}\int_0^t \varepsilon_R(\tau)d\tau, \qquad 4.\ 14$$

$$\sigma = \frac{A}{A_s}E\varepsilon_t. \qquad 4.\ 15$$

The modulus used for the aluminum pressure bars was $10\text{x}10^6$ psi, the density used was $2.53\text{x}10^{-4}$ (lb in/s)/in^3. The calculated wave velocity (C_0) was $1.99\text{x}10^5$ in/s. The bar diameter (A) was 0.5 inches. The properties of the specimen's length (L) and area (A_s) varied a little between each specimen but the average length was 0.08 inches and the average area was 1.57 in^2.

To check for uniform stress distribution the technique discussed in section 2.4.4 were employed. Equation 2.18 was used to calculate the stress at the incident side of the specimen. This stress was compared to the stress calculated from equation 4.16. An example of this plot is shown in figure 4.31. In this graph "Stress T" is the stress obtained from the transmission side of the specimen and "Stress I+R" is the stress obtained from the incident side of the specimen. Because of the nature of polyurethane it was difficult to obtain smooth curves for an accurate stress comparison. The oscillations seen in the figure below are due to read error rather than actual oscillations seen by the specimen.

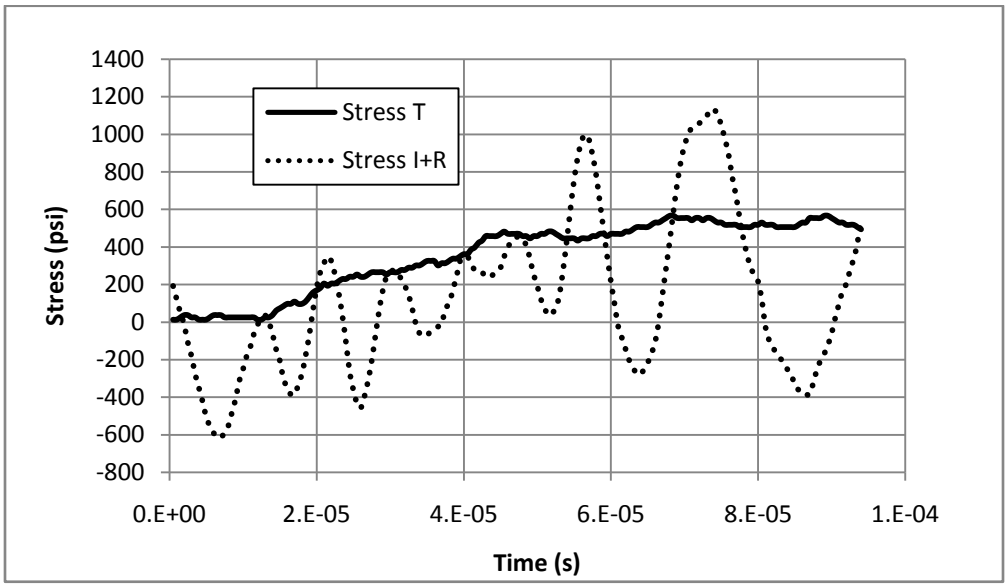

Figure 4.31 A Comparison of the Stress at Both Sides of Polyurethane Specimen

In order to obtain an accurate stress strain curve the stress and strain needed to be aligned properly. To do this the reflected and transmitted strain waves were plotted on the same graph and aligned visually. The effect of misalignment is small. The alignment is accurate to plus or minus $2x10^{-6}$ seconds. The effect of misalignment on the stress-strain

curve is shown in figure 4.32. For this figure an intentional misalignment was given to demonstrate the effect of misalignment on the stress-strain curve. For polyurethane the stress-strain curve is not sensitive to the alignment of the reflected and transmitted curves.

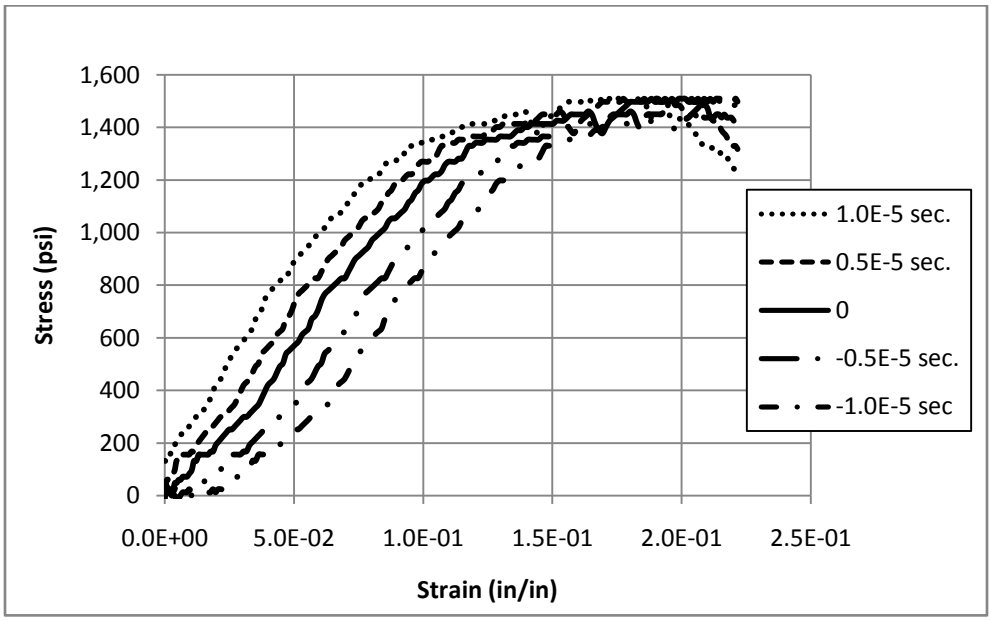

Figure 4.32 Misalignment of Incident and Reflected Strain Signals for Polyurethane

Based on the visual alignment of the curves the stress and strain were plotted together to form a stress strain curve, an example curve is shown in figure 4.33. The strain rate versus the strain was also plotted to show what the strain rate was for a given stress and strain.

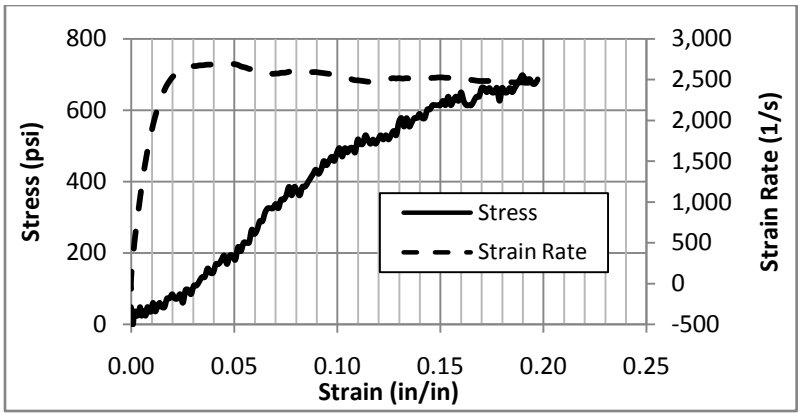

Figure 4.33 Stress and Strain Rate Compared to Strain for a Single Polyurethane Test

The stress strain curve is not smooth in figure 4.33. This is due primarily to the low signal to noise ratio in the transmitted wave. The transmitted wave had very low amplitude which meant the noise observed had a large impact on the stress. Because of effect of noise on the signal several specimens were tested for each ball model.

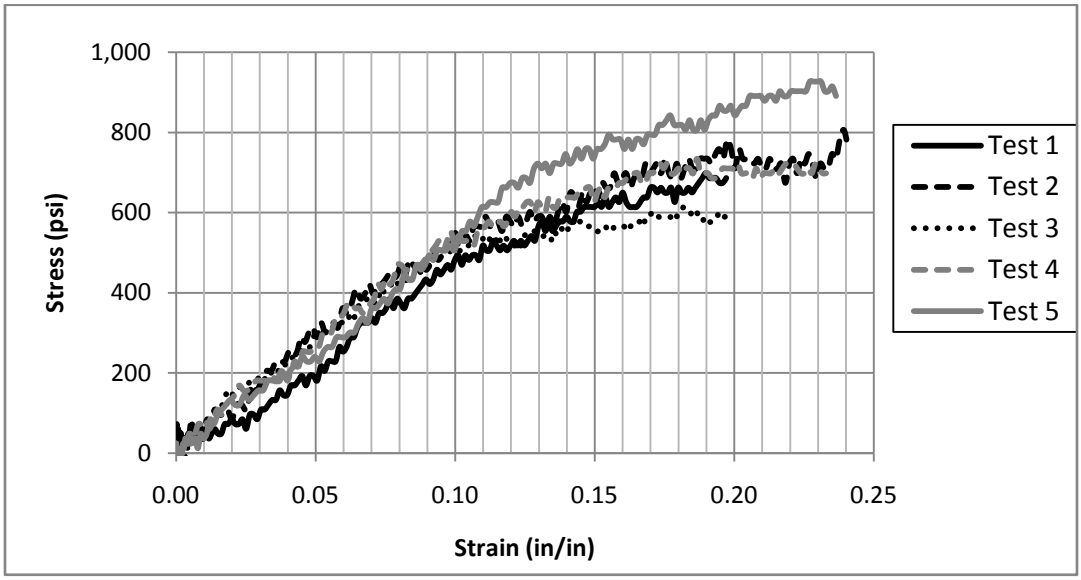

Figure 4.34 High Strain Rate Data for SX44RLA3, Stress-Strain Curves Used for Averaging

The strain rate is controlled by two main factors, the speed of the striker bar and the thickness of the specimen. The 9 inch striker bar was fired using a tank pressure of 5 psi. It was found that a tank pressure of 5 psi was needed to attain a sufficient velocity for the striker bar to reach the end of the cannon barrel. To attain a lower strain rate a thicker sample would be needed. Because of difficulty in obtaining transmitted signals with thicker specimens a thin specimen was used. For these reasons it would be difficult to obtain stress strain curves with this SHPB at lower strain rates.

The high strain rate stress-strain behavior of softballs were obtained for softballs with varied COR values. The stress-strain behavior of the balls is shown in figure 4.35. It was expected that the COR would not have an effect on the loading of the stress-strain curve because it is a measure of rebound. This lack of change in the behavior is noticeable. As expected the behavior changed very little based on the change in COR values. The .43/5606 ball has a larger stress for a given strain.

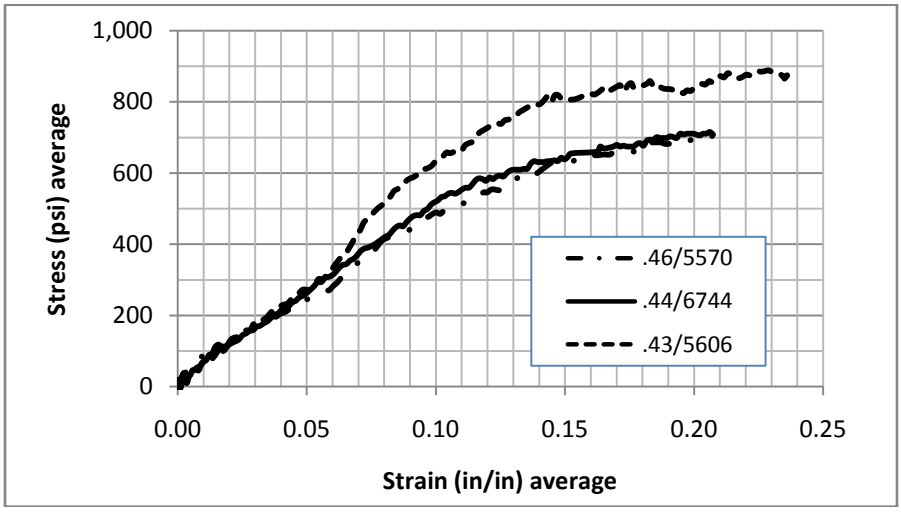

Figure 4.35 Stress-Strain Curve at Strain Rate of 2780 s^{-1} for Varied COR Softballs

The high strain rate behavior of varied DS balls was also measured. It was expected that as DS increased the response of the softball would also increase. This can be observed in figure 4.36. As the DS increased the response of the softball increased.

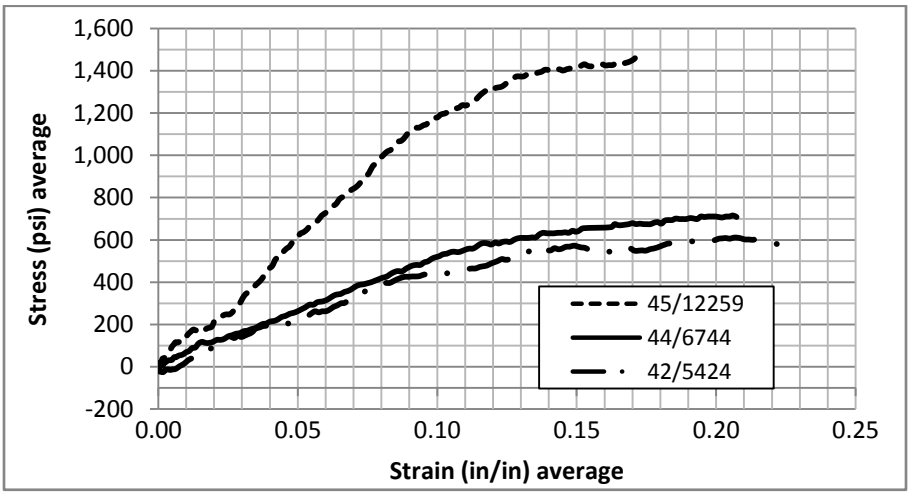

Figure 4.36 Stress-Strain Curve at Strain Rate of 2780 s^{-1} for Varied DS Softballs

In each of the high strain rate tests there is a fairly linear region between 0 and 0.1 strain. The slope of the linear section in each ball is the high strain rate modulus. The high strain rate modulus for each ball is shown in table 4.7.

Table 4.7 High Strain Rate Modulus

Manufacturer	Model	COR	DS (lbs/in)	High Strain Rate Modulus (psi)
Dudley	WT11 ND Y-1	0.45	12259	12158
Diamond	12RSC 44	0.42	5424	4191
Worth	SX44RLA3	0.44	6744	5114
Diamond	12RFPSC 47	0.46	5570	4796
Diamond	12RSC 40	0.43	5606	6104

There was a trend noticed in the high strain rate modulus of the varied DS balls. As the DS increased that high strain rate modulus increased, the increase was not linear.

This trend is shown in figure 4.37. This trend demonstrates the expected increased response seen in figure 4.36.

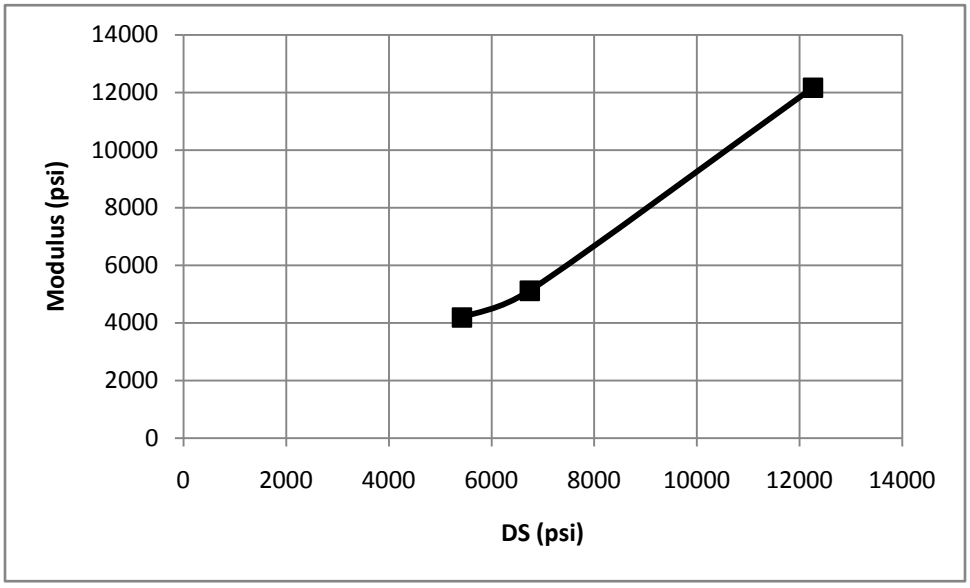

Figure 4.37 High Strain Rate Modulus with Varied Stiffness

There is a slight downward trend associated with the high strain rate modulus of varied COR softballs. The trend is probably a result of the variations in the DS of the balls used since there was a demonstrated trend associated with DS and the DS of the softballs points to the downward trend shown in figure 4.38.

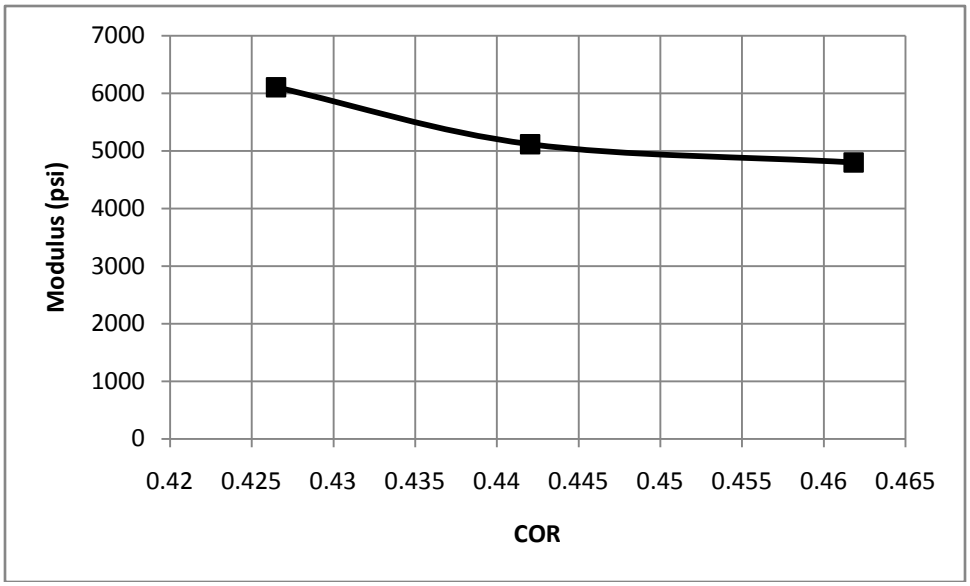

Figure 4.38 High Strain Rate Modulus with Varied COR

4.7 Discussion

4.7.1 Stress Increase with Strain Rate

Polyurethane is a viscoelastic martial. Using a viscoelastic model it has been shown in section 4.4.4 that the properties of viscoelastic materials are rate dependent. Based on this rate dependence the data obtained during the low strain rate test should be lower than the data obtained during the high strain rate test. Figure 4.39 compares the stress strain behavior measured during the two tests.

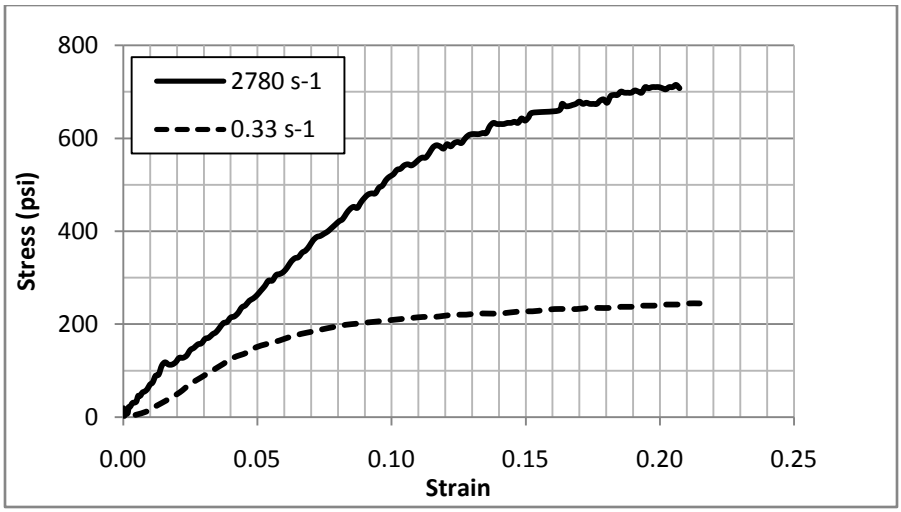

Figure 4.39 Stress Strain Curve Strain Rate Comparison for 44/375 Ball

It can be seen in figure 4.39 that there is an increase in the slope of the curve as strain rate increases. This increase was seen on all five ball models. The graphs of the other four balls are shown in Appendix B. The increase at 0.2 strain for each ball model is shown in table 4.8. The average increase at 0.2 strain is 42%. For most of the balls the strain at 0.2 is on the plateau of the stress strain curve. This gives a comparison of the stress increased needed to reach the plateau due to increased strain rate.

Table 4.8 Stress Change at 0.2 Strain Between Strain Rates of 2780 s^{-1} and 0.33 s^{-1}

Manufacture	Model	COR	DS (lbs/in)	% Change
Dudley	WT11 ND Y-1	0.45	12259	48%
Diamond	12RSC 44	0.42	5424	41%
Worth	SX44RLA3	0.44	6744	34%
Diamond	12RFPSC 47	0.46	5570	42%
Diamond	12RSC 40	0.43	5606	47%

4.7.2 Modulus Increase with Strain Rate

The modulus was calculated for the tests conducted at strain rates of 0.33 s^{-1} and 2780 s^{-1}. The modulus for the low strain rate tests are shown in table 4.5 and the modulus for the high strain rate tests are shown in table 4.7. The percent change in modulus for each ball is shown in table 4.9. The average increase in modulus is 33%. This can be seen in figure 4.40 and figure 4.41 where the modulus with varied comp. and COR are graphed for high strain rate and low strain rate. The downward trend associated with the varied COR could be due to the variations in the DS of those softballs.

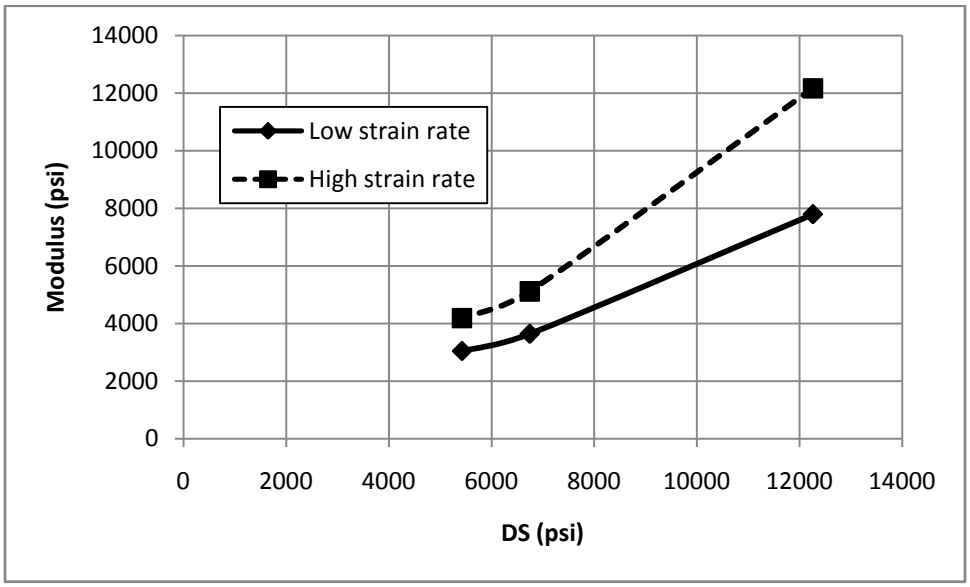

Figure 4.40 High and Low Strain Rate Comparison for Varied Stiffness

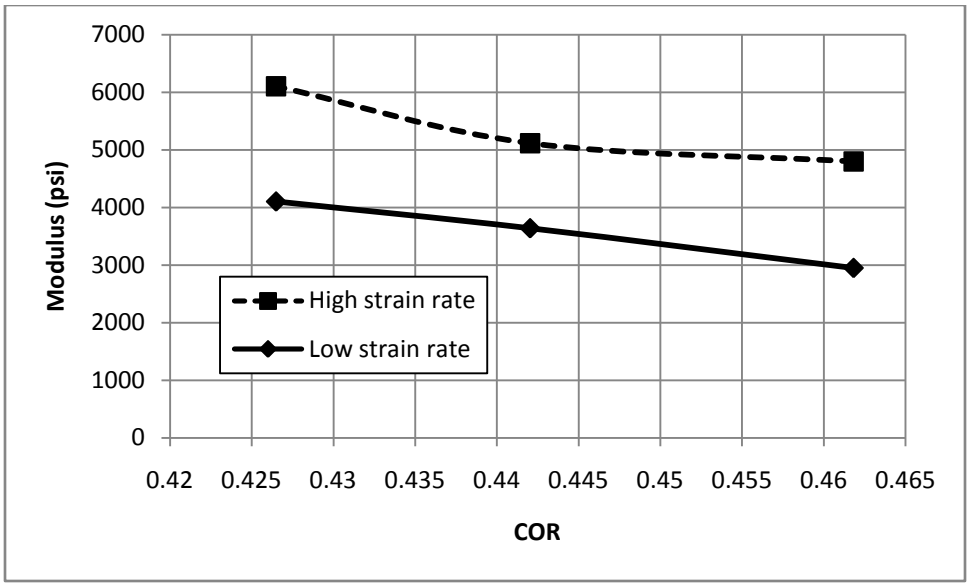

Figure 4.41 High and Low Strain Rate Comparison for Varied COR

Table 4.9 Modulus Percent Increase Due to Increased Strain Rate

Manufacturer	Model	COR	DS (lbs/in)	%
Dudley	WT11 ND Y-1	0.45	12259	36%
Diamond	12RSC 44	0.42	5424	27%
Worth	SX44RLA3	0.44	6744	29%
Diamond	12RFPSC 47	0.46	5570	39%
Diamond	12RSC 40	0.43	5606	33%

4.7.3 Viscoelastic Comparison

The viscoelastic stress-strain response is dependent on the dynamic stiffness of softballs. This is shown in figure 4.15. These viscoelastic models used in finite element models have had problems matching the observed behavior of softballs when the velocity of impact is changed. A comparison between the viscoelastic model and the high strain rate data is desired.

The measured stress strain behavior can be compared to the behavior predicted by the viscoelastic model. The curves for the viscoelastic model are calculated with a strain rate of 2500 s^{-1}. The average strain rates for the curves tested with the SHPB are 2780 s^{-1}. A comparison between SX44RLA3 and the viscoelastic models are shown in figure 4.42.

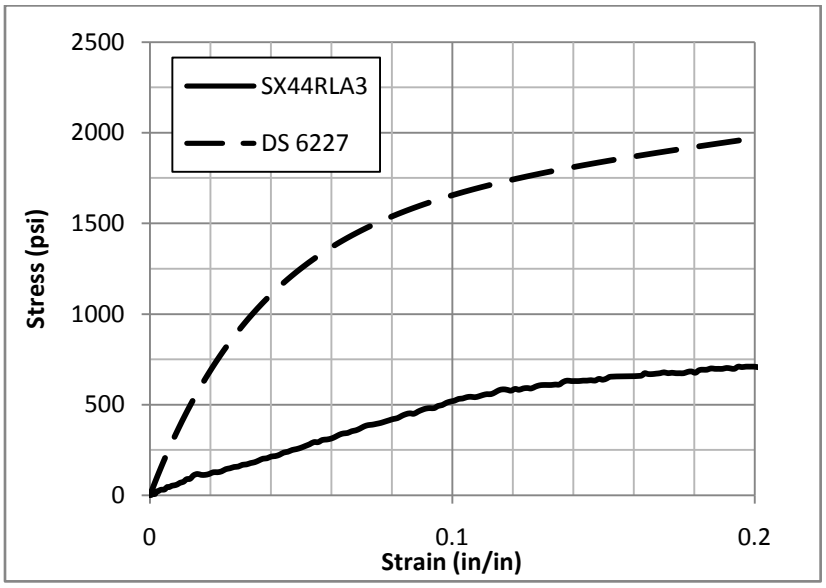

Figure 4.42 .44/375 Ball Compared to the Viscoelastic Model

Since the DS of the SX44RLA3 ball is 6744 it should be above the viscoelastic curve for DS 6227 not below. The other softball models are also graphed with the closest DS curve. These graphs are shown in Appendix C. The viscoelastic model is over predicting the amplitude of the stress strain curve. This could be why the viscoelastic model is not matching up with the data observed.

The strain rate is changing throughout the impact of the softball. The curve in figure 4.12 peaks around 2500 s^{-1} , but this is only for a small amount of time. The coefficients used in the ball model were obtained experimentally in laboratory test. The

viscoelastic model when used in an FEA model predicts the performance of the bat and ball quite well at the speeds the coefficients were obtained at. Because of this there is some confidence in the viscoelastic model. Also the high strain rate behavior the model is compared to was measured with and is believed to be accurate.

Using a strain rate that varies with time could help in matching the behavior of material obtained at high strain rates. This was done for SX44RLA3 shown in figure 4.43. The average strain rate measured from the test was used as the *R* term in the viscoelastic model. This is shown in figure 4.43 as the dotted line. This prediction of the viscoelastic model is still over predicting the measured behavior of the softball.

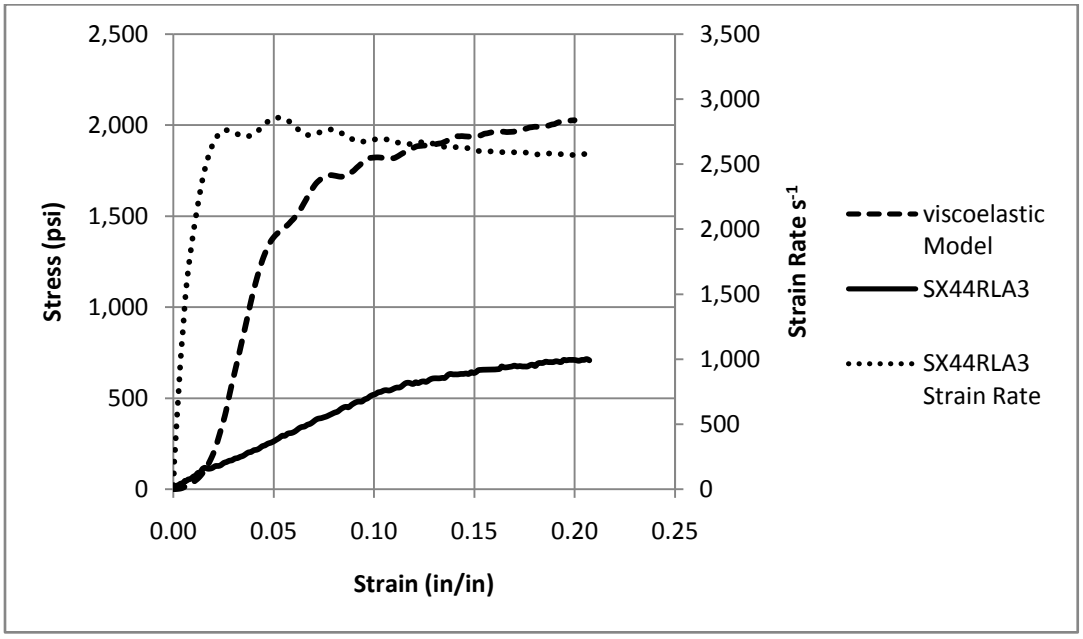

Figure 4.43 Viscoelastic Comparison Using Varied Strain Rate.

Since the ball impact is at the high strain rates for a short time the viscoelastic model may predict the balls behavior at a much lower average strain rate. The average strain rate based on the data shown in figure 4.13, the average strain rate the ball sees is

around 1000 s^{-1}. The high strain rate data is graphed with the viscoelastic model for several different strain rates in figure 4.44. By adjusting the strain rate *R* term the measured stress-strain curve cannot be matched, also the measured data has a strain rate of 2780 s^{-1}. In order to match the curves measured the other parameters in the viscoelastic model need to be adjusted.

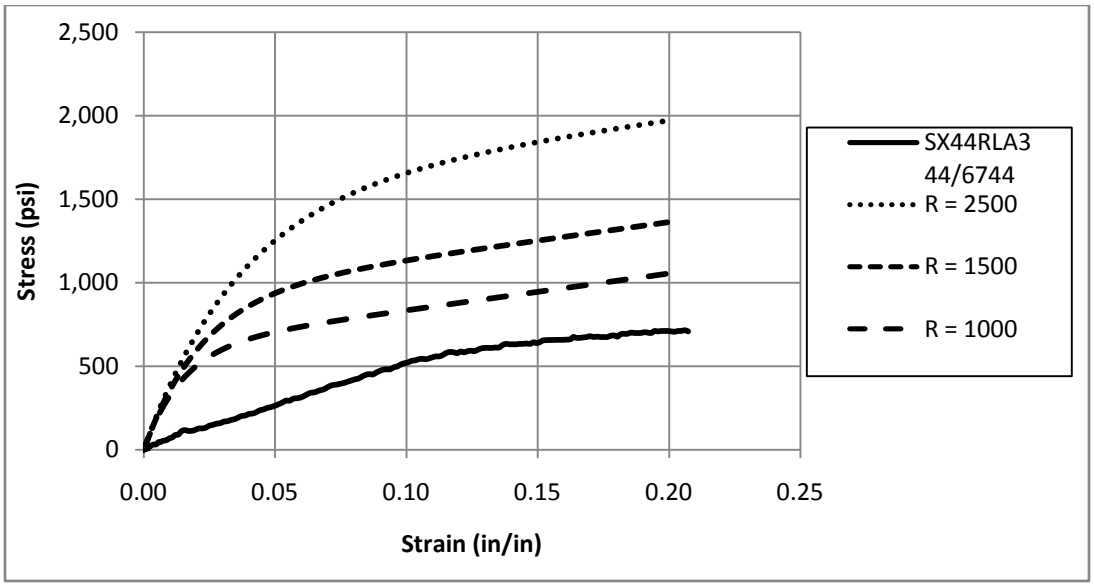

Figure 4.44 Viscoelastic Strain Rate Variation Compared to High Strain Rate Data for SX44RLA3

To consider how a viscoelastic model might describe the measured ball response, the viscoelastic parameters were varied to fit the measured response as shown in figure 4.45 - figure 4.49, the parameters used are shown in table 4.10.

Table 4.10 Viscoelastic Model Adjusted Parameters

Model	DS (lbs/in)	R (1/s)	G_∞ (psi)	Go (psi)	β	ν
WT11NDY-1	12259	2780	400	10000	40000	0.1
12RSC44	5424	2780	400	3500	40000	0.1
SX44RLA3	6744	2780	400	4200	40000	0.1
12RFPSC47	5570	2780	400	4000	40000	0.1
12RSC40	5606	2780	400	5200	40000	0.1

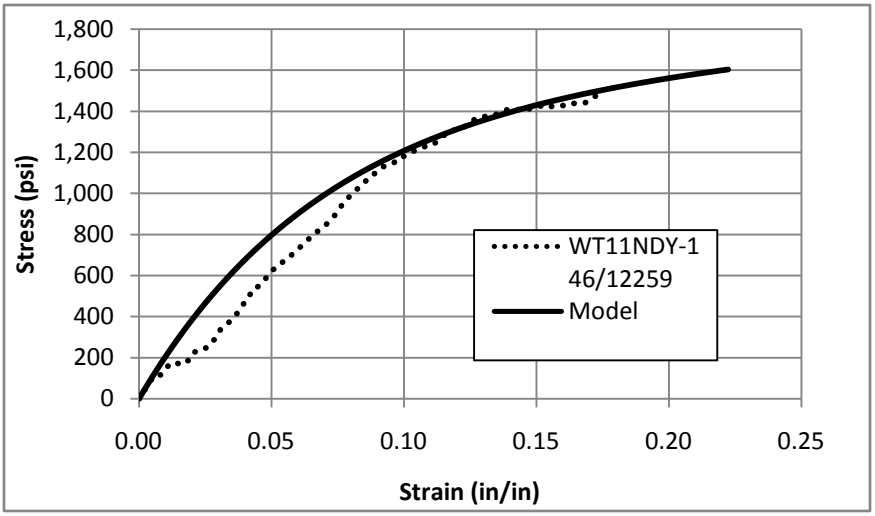

Figure 4.45 Viscoelastic Model of WT11NDY-1 46/12259

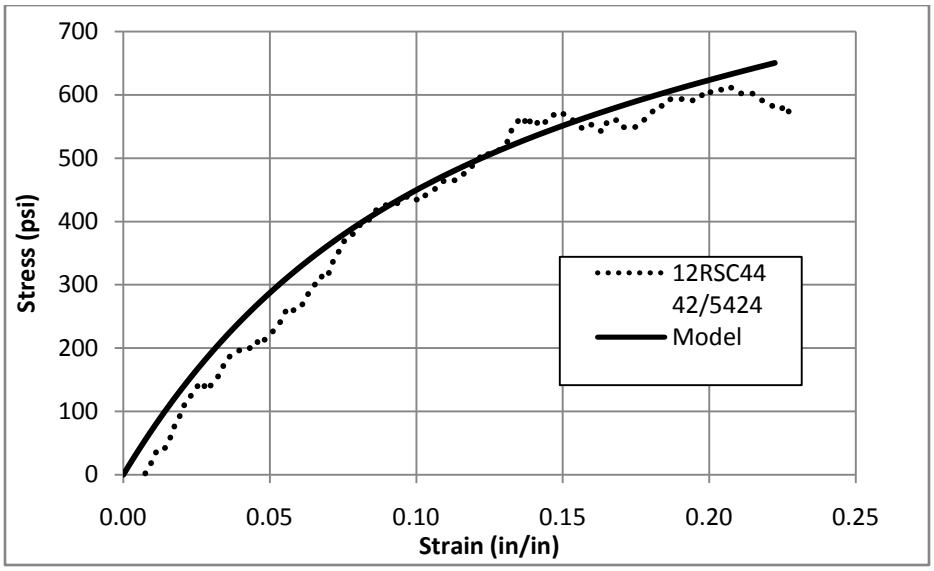

Figure 4.46 Viscoelastic Model of 12RSC44 42/5424

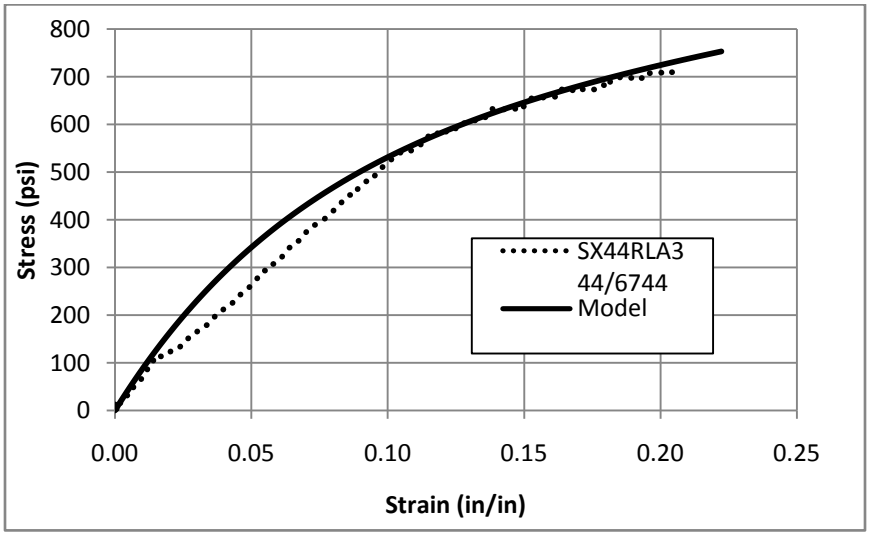

Figure 4.47 Viscoelastic Model of SX44RLA3 44/6744

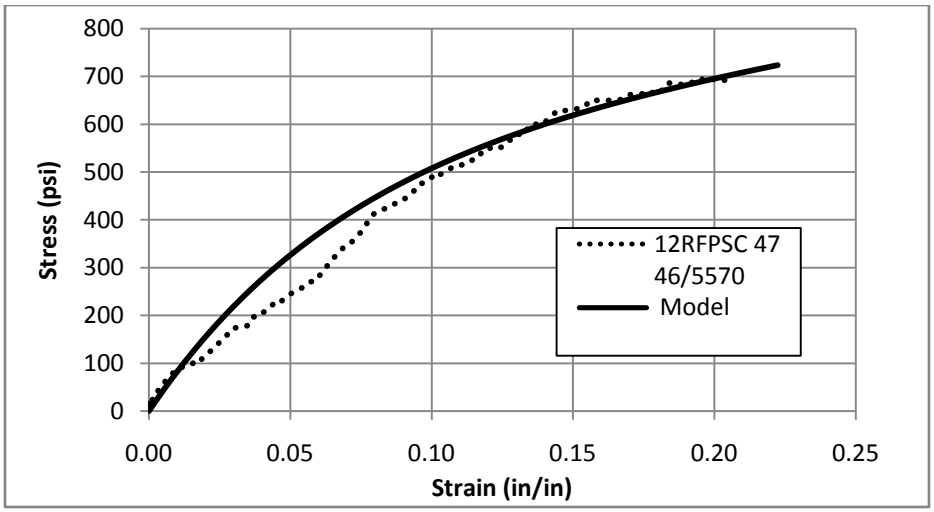

Figure 4.48 Viscoelastic Model of 12RFPSC47 46/5570

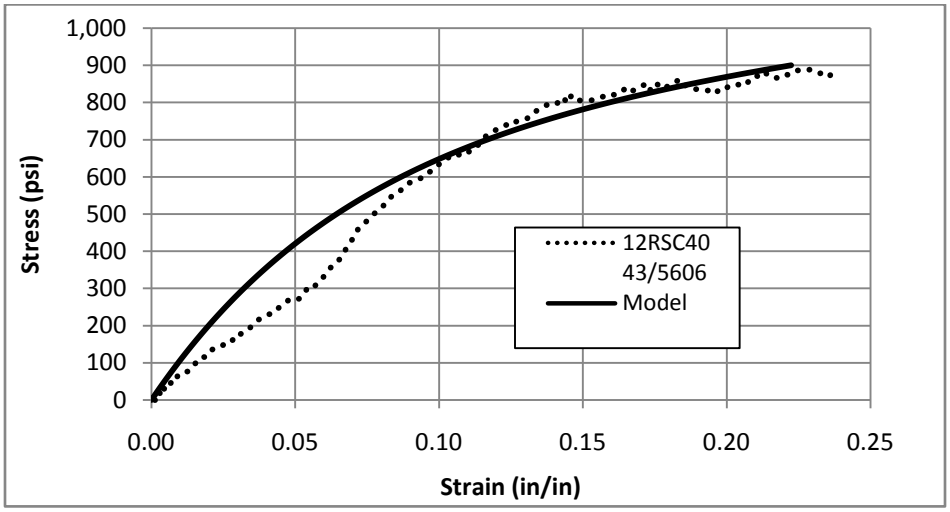

Figure 4.49 Viscoelastic Model of 12RSC40 43/5606

4.8 Summary

To compare effects of varied stiffness and rebound properties in softballs several tests were done. Tests at high strain rates, as well as tests at low strain rates were conducted.

The split Hopkinson pressure bar setup was verified with the testing of Nylon 6/6. The data collected for Nylon 6/6 was compared to data published for Nylon 6/6. It was found that the published data and the measured were quite close.

The capabilities of the split Hopkinson pressure bar were discussed. The pressure supplied to the cannon controlled the velocity of the striker bar. It was found that with increased velocity the amplitude of the incident stain increased.

The duration of the incident pulse was found to be related to the striker bar length. With increased length of the striker bar the pulse duration increased. Because of the increased mass in longer striker bars the pressure had to be adjusted to attain the same velocity. An equation was developed to approximate the pressure needed for the different striker bars to reach the same velocity.

Different shaping techniques were discussed. Tapered tips were used to try and change the shape of the incident wave. It was found that these tips introduced more error and variations in the readings. Another method investigated to shape the incident wave was the use of shaping samples between the striker bar and the incident bar. In this case it was also found that the wave shaping caused more error and variations.

In the testing of polyurethane samples it was found that the length had a significant impact on the ability to record a transmission wave. With longer samples the transmission wave could not be distinguished from the line noise. By reducing the sample length a larger amplitude transmission wave was recorded.

Comparing the cell size under magnification it was determined that as compression increases the cell size also increased. It was also noted that for increased COR the cell size increases.

A finite elements model was constructed and run by a third party. It was found that the predicted strain rate that the ball sees is around 2500 s^{-1}. The strain at this point is about 0.2. These predictions from the finite elements model were the target for the high strain rate tests.

The viscoelastic model used in the finite elements model was looked at. The stress and strain were graphed for different dynamic stiffness balls. A strain rate of 2500 s^{-1} was used to construct these graphs.

Low strain rate tests were conducted to determine the stress strain behavior of the rigid polyurethane foam. It was found that the slope of the stress strain graph starts out linear. After the linear section the slope reduces for the majority of the deformation. At larger strain the slope increases again. The modulus of the first section of the stress strain graph was compared for the different ball models. It was found that the modulus decreases with increased COR, and increases with increased stiffness. The hysteresis of the ball models were also looked at. It was found that there was no trend for the hysteresis of the balls based on COR, but it was found that the hysteresis increased with increased stiffness.

The different softball models were cut and thin specimens were constructed from each ball. These specimens were tested in the split Hopkinson pressure bar. It was found that even though thin specimens were used the signal to noise ratio still was a problem.

Because of noise interference six tests were averaged for each ball model. The averaging cleaned up the signals resulting in good curves. It was found that the COR did not seem to have much of an impact on the stress strain at high strain rates. The stress strain behavior was dependant on the comp of the balls.

It was found that the stress increased with strain rate. This was seen in all the ball models. The increase in stress was measured at 0.2 strain and the average was found to be 42%. The modulus also increased with increased strain rate. The modulus increased by an average of 33% for all ball models.

Comparing the high strain rate stress and strain with the viscoelastic model it was found that the viscoelastic model was greater than the measured stress and strain. The viscoelastic model parameters were changed to fit viscoelastic stress-strain curve to the measured high strain rate stress-strain curve.

5 Summary and Future Work

5.1 Summary

The impact properties of polyurethane are important because of their use in softballs. Several different softball models with different stiffness's and rebound properties were tested. These samples were tested at high strain rates.

An effective way of testing materials at high strain rates is with a split Hopkinson pressure bar. The setup consists of two pressure bars with strain gages mounted in the centers of each bar. The specimen is sandwiched between the two pressure bars and a striker bar is fired at one end. This causes a compression wave to travel down the pressure bars. Part of this wave is reflected and transmitted at the specimen. The strain gages record the waves. Data reduction techniques are used to calculate the stress, strain and strain rate in the specimen.

In order to test the polyurethane at high stain rates a split Hopkinson pressure bar was built. The pressure bars were made of aluminum allowing for better signal transmission with soft materials. These aluminum bars were instrumented with strain gages connected to conditioners. A computer was connected to the setup and a program was used to control the setup and record the strain readings.

The velocity of the striker bar was controlled with the pressure in the supply tank. It was found that with increased pressure the signal read by the incident strain gage increased. The duration of the strain was found to be related to the striker bar length. An increased length corresponded to and increased duration.

A finite element model was used to estimate what the strain rate and stain amplitude were during a softball impact. These values were used as the target values for the high strain rate tests. The viscoelastic model used for generating the data in the finite elements model was graphed for different balls. This was later compared to the data obtained from the highs strain rate tests.

Tests were conducted to determine the base low strain rate behavior. The stress strain curve was plotted for all the ball models investigated. It was found that the modulus decreased with increased COR and increased with increased stiffness. The hysteresis effect of the ball was also tested at low strain rates. It was found that COR had no impact on hysteresis and the stiffness caused an increase in stiffness..

For the high strain rate testing thins specimens were constructed and tested in the split Hopkinson bar apparatus. Averaging six tests for each ball model good stress strain curves were obtained. It was found that the stress strain behavior was affected by the stiffness much more than the COR.

Comparing low strain rate curves with high strain rate curves it was found that an increased strain rate corresponded to an increase in stress and modulus. It was also found that the stress in the viscoelastic model was much higher than the measured stress. The viscoelastic model parameters were changed to fit the measured data. Although the model did not match the data measured it worked for modeling the ball properties seen in laboratory tests. This could be because the ball only experiences high strain rates for a short period of time and the model is used for high strain rates.

5.2 Future Work

Based on the disagreement between the viscoelastic models and the measured impact properties of the softball future work is needed to accurately model the behavior of the softball. It would be beneficial to have the measured properties of the softball at the average strain rate obtained from the bat-ball impact. Testing at this strain rate with the SHPB setup discussed in this thesis was not possible due to the constraints of the sample length and striker bar minimum speed.

It may help to do some modifications to the SHPB cannon to enable slower striker bar speeds. It could also be beneficial to install load cells on either side of the sample similar to the ones Chen used (7). If these adjustments to the SHPB don't allow for testing at the average impact strain rate then a drop test might help. It may also be helpful to make adjusts in the viscoelastic model that match the tested data and accurately model the ball in the FEA model.

6 References

1. **Duris, Joseph.** *Experimental and Numerical Characterization of Softballs.* Washington State University. 2004.

2. **Faber, W.** *Finite Element Modeling of Softballs.* 2009. Personal Communication.

3. **Gray III, GT.** Classic Split-Hopkinson Pressure Bar Testing. *ASM Handbook.* Materials Park : ASM International, 2000, Vol. 8, pp. 462-476.

4. *High-strain-rate compressive behavior of a rigid polyurethane foam with various densities.* **Chen, W, Lu, F and Winfree, N.** 2002, Exp Mech, Vol. 42, pp. 65-73.

5. *An Investigation of the Mechanical Properties of Materials at very High Rates of Loading.* **Kolsky, H.** 1949, Proceedings of the Physical Society of London, Vol. 62, pp. 676-700.

6. *A Polymeric Split Hopkinson Pressure Bar Instrumented with Velocity Gages.* **Casem, DT, Fourney, WL and Chang, P.** 2003, Soc for Exp Mech, Vol. 43, pp. 420-427.

7. *Dynamic Compression Testing of Soft Materials.* **Chen, W, et al.** 2002, J Appl Mech, Vol. 69, pp. 214-223.

8. **Kaiser, MA.** Advancements in the Split Hopkinson Pressure Bar Test. *Virginia Polytechnic Institue and State University.* [Online] 1998. http://soar.wichita.edu:8080/dspace/bitstream/10057/775/1/t05035.pdf.

9. **Gray III, GT and Blumenthal, WR.** Split-Hopkinson Pressure Bar Testing of Soft Materials. *ASM Handbook.* Materials Park : s.n., 2000, Vol. 8, pp. 488-496.

10. *Split Hopkinson Pressure Bar Techniques for Characterizing Soft Materials.* **Song, B and Chen, W.** 2005, Latin American Journal of Solids and Structures, Vol. 2, pp. 113-152.

11. *On the use of the Compression Split Hopkinson Pressure Bar to High Strain Rate.* **Couque, H and Walker, JD.** 1994, Journal de Physique, Vol. 4, pp. 23-28.

12. *A Method of Measuring the Pressure Produced in the Detonation of High Explosives or by the Impact of Bullets.* **Hopkinson, B.** 1914, Proceedings of the Royal Society of London, Vol. 89, pp. 411-413.

13. *High Strain-rate Testing: Tension and Compression.* **Lindholm, US and Yeakley, LM.** 1968, Experimental Mechanics, Vol. 8, pp. 1-9.

14. *On the Use of Electrical-Resistance Foil Strain Gages for Plastic-Wave Studies in Solids.* **Khan, AS and Hsiao, C.** 1988, Experimetal Mechanics, Vol. 28, pp. 254-258.

15. *The Effect of Strain Rate and Heat Developed During Deformation on the Stress-Strain Curve of Plastics.* **Chou, SC, Robertson, KD and Rainey, JH.** 1973, Exp Mech, Vol. 13, pp. 422-432.

16. *A Three Dimensional Analytical Solution of the Logitudinal Wave Propagation in an Infinite Linear Viscoelastic Cylindrical Bar.* **Zhao, H and Gray, G.** 1995, J. Mech. Phys. Solids, Vol. 43, pp. 1335-1348.

17. **Backus, JK.** Rigid Polyurethane Foams. [ed.] D Klempner and KC Frisch. *Polymeric Foams.* New York : Oxford Univeristy Press, 1991, 5, pp. 73-94.

18. **Smith, Kathy.** *Softball Manufacturing Techniques.* July 21, 2009. Personal Communication.

19. **Tasneem, N.** Study of the Wave shaping techniques of the Split-Hopkinson Pressure Bar Using Finite Element Analysis. *Witchita State University.* [Online] 2005. http://soar.wichita.edu:8080/dspace/bitstream/10057/775/1/t05035.pdf.

20. **Gibson, Ronald F.** Analysis of Viscoelatic and Dynamic Behavior. *Principles of Composite Material Mechanics.* Second Edition. Boca Raton : CRC Press, 2007, pp. 377-464.

21. *The Velocity of Longitudinal Waves in Cylindrical Bars.* **Bancroft, D.** 1941, Physical Review, Vol. 59.

Appendix A

How to operate the Sport Science Lab Split Hopkinson Pressure Bar

The following are instructions on how to operate the SHPB that was built for this thesis. These are the procedures that were followed for obtaining the data used for this thesis.

Boot up and turn on procedure

There are several power strips and switches that need to be turned on for the proper operation of this pressure bar. The following are the order that things should be turned on. Refer to Figure A.1 for the placement of switches.

1. Power strip located on the back of the frame should be turned to the ON position.
2. Turn the computer on and allow it to boot up.
3. Open LabView and select “Pressure Bar.vi” from the list of recently opened vi’s.
4. Make sure the black switch located on the right front leg is in the on position.
5. Twist the red safety switch on.
6. Make sure both conditioners are on and the voltage is zeroed for both strain gages.

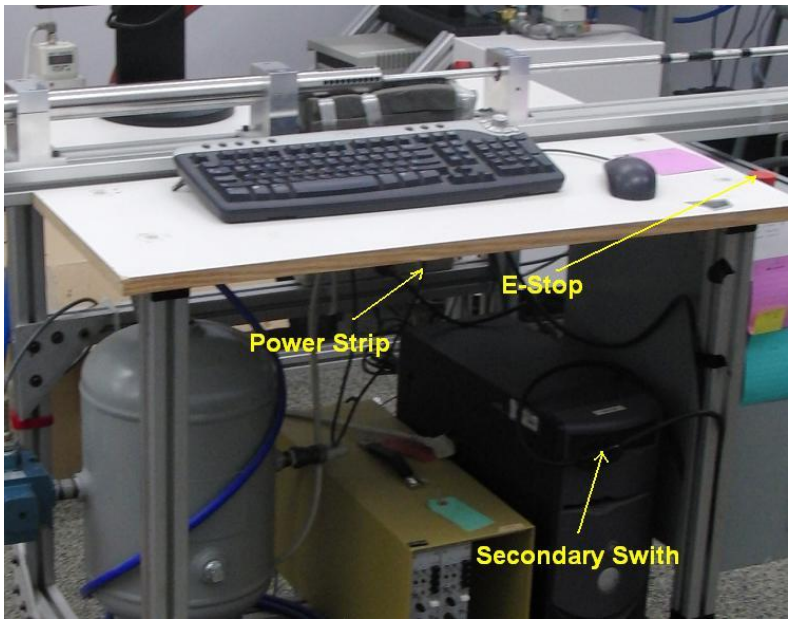

Figure A.1 SHPB Switches

Pressure bar front panel operation

Now that the power is on and the computer is running, the LabVIEW software needs to be opened. To run the LabVIEW program follow the steps below. Fig is a screen shot of the LabView front panel.

1. Go to start and click on LabVIEW. This should open the program.
2. Select “Pressure Bar.vi” from the list of vi’s. This should open the control panel for the split Hopkinson pressure bar.
3. Create a new summery file and wave file for saving the data.
4. Click on the folder button next to the summery file or wave file.
5. Create a new text document for each.
6. Select the newly created text document for the summery file and wave file.
7. Input the bar properties under the bar properties section.

8. Under the sample properties section put in the length and diameter of the sample.
9. Next set the tank pressure. If the tank pressure is too high it could damage the bars and if it is too low the bar won't make it to the end of the cannon barrel. It is suggested to use a pressure between 5 and 10 psi.
10. Select an appropriate frequency and number of samples. These fields are located above the "Strains" graph to the right of the screen.
11. Click the run button in the top left corner. It is a white arrow.
12. Care should be taken not to fire the bar while it is being loaded.

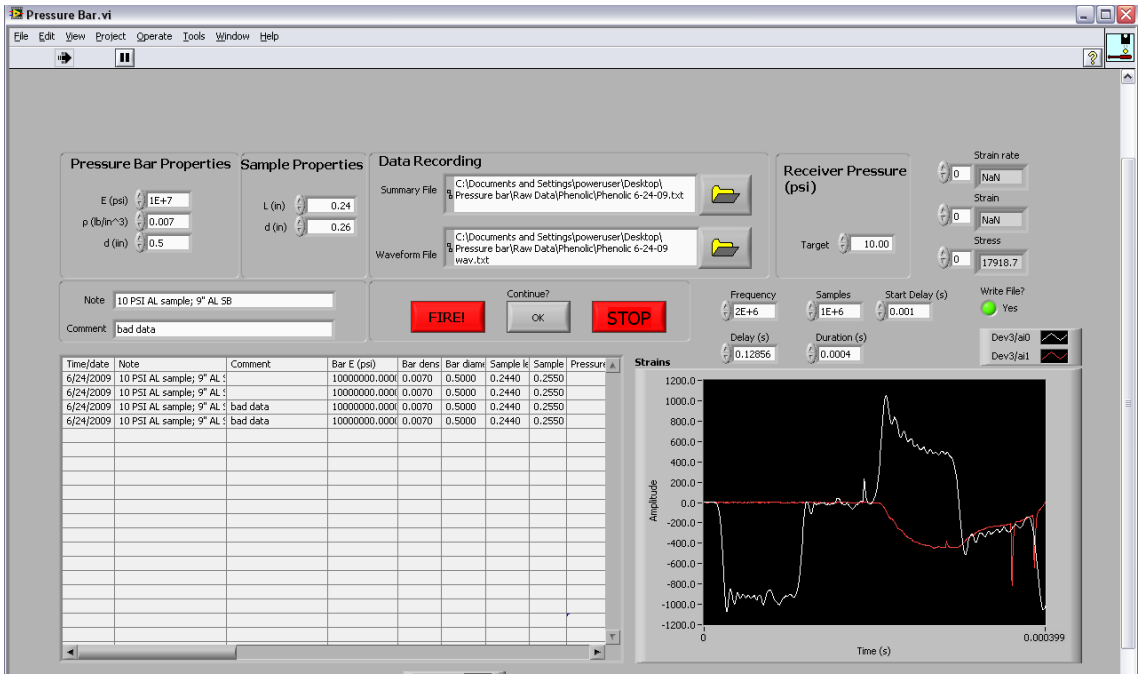

Figure A.2 Pressure Bar VI Front Panel

Pressure bar firing procedure

Once the above is completed the pressure bar should be ready to fire. The following is the firing procedure for the SHPB.

1. Select the appropriate striker bar.
2. Load striker bar into barrel and use loading rod to push to the back of the barrel.
3. Apply a thin film of grease between the barrel and the incident bar.
4. Apply a thin film of grease between the specimen and both the incident and transmission bar.
5. Place the specimen between the incident and transmission bars. It should stick to either bar due to the grease on the bar ends.
6. Place container under specimen and cover the specimen to prevent the specimen from flying around the room.
7. Make sure the incident bar is very close to the barrel opening and that both bars are contacting the specimen.
8. Press FIRE in the LabView window.

Appendix B

Below are graphs comparing high strain rate stress strain curves with low stress strain curves for the softballs that were tested. The graph of the other ball that was tested is shown in figure 4.39.

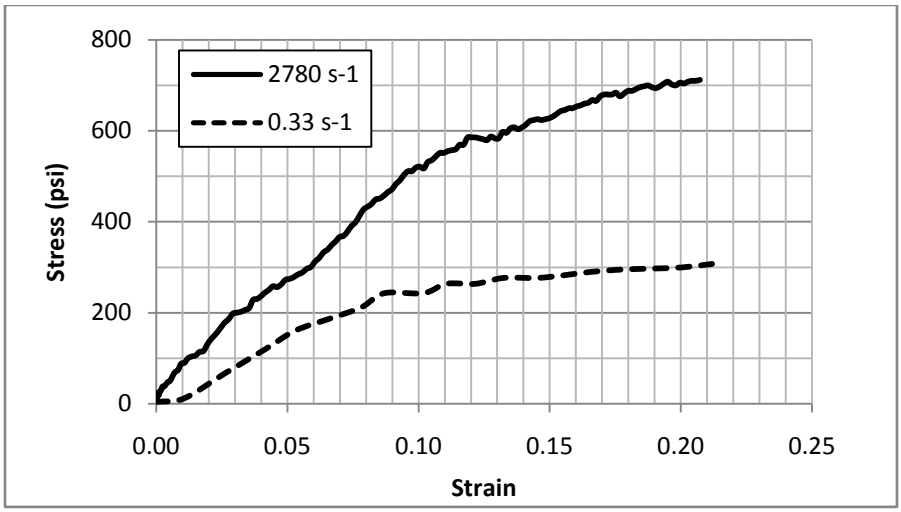

Figure B.1 Stress Strain Curve Strain Rate Comparison for 47/375 Ball

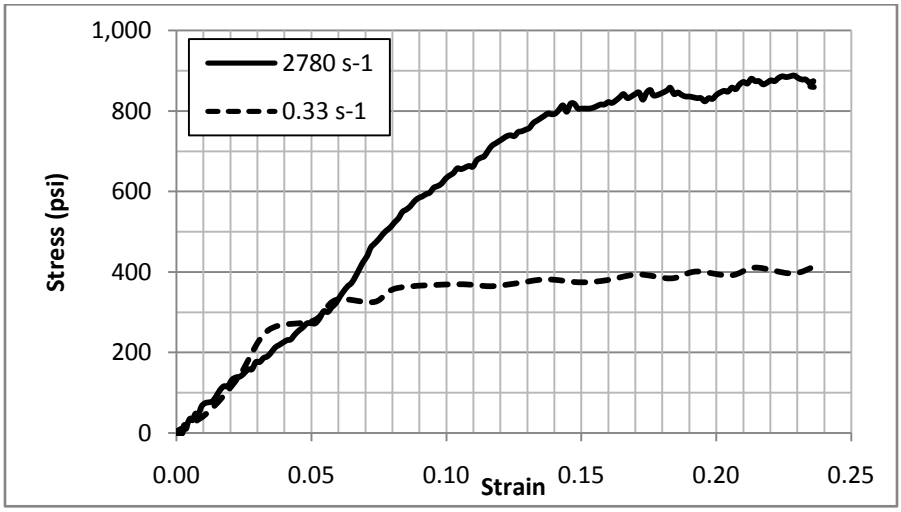

Figure B.2 Stress Strain Curve Strain Rate Comparison for 40/375 Ball

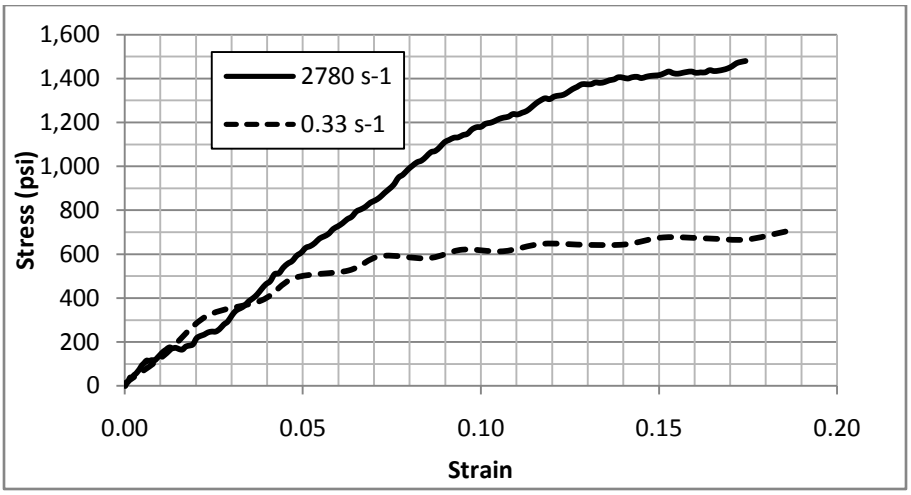

Figure B.3 Stress Strain Curve Strain Rate Comparison for 44/525 Ball

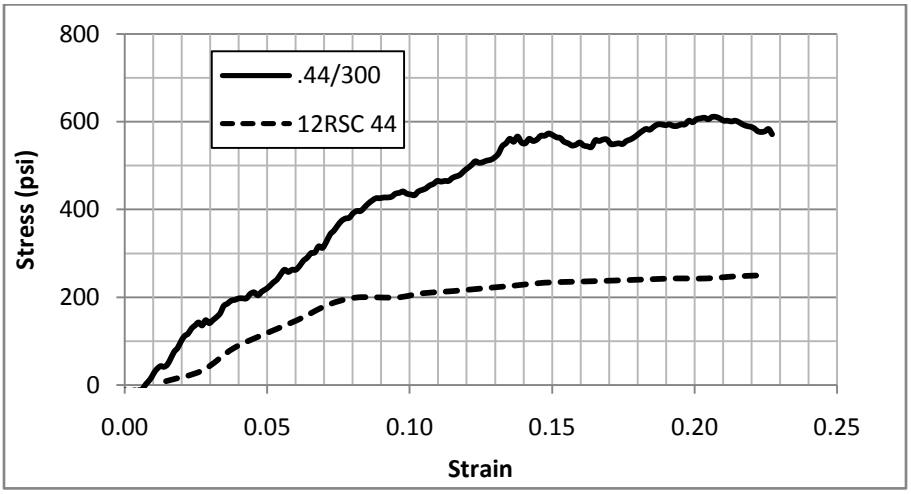

Figure B.4 Stress Strain Curve Strain Rate Comparison for 44/300 Ball

Appendix C

Graphs of the high strain rate SHPB tests are compared to the viscoelastic model. The viscoelastic model has a strain rate of 2500 s^{-1}. The parameters used for modeling the viscoelastic behavior can be found in table 4.4. The high strain rate SHPB test had an average strain rate of 2780 s^{-1}. The other graph that goes with this section is figure 4.42.

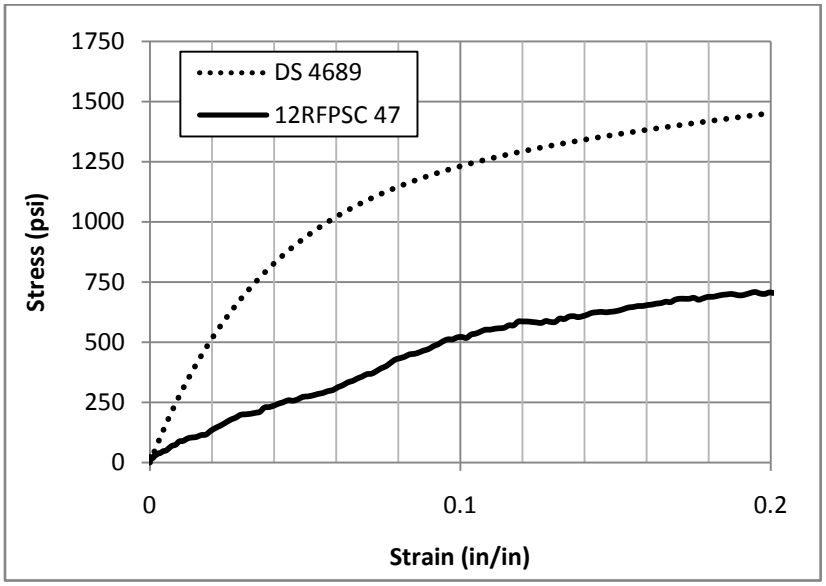

Figure C.1 .47/375 Ball Compared to the Viscoelastic Model

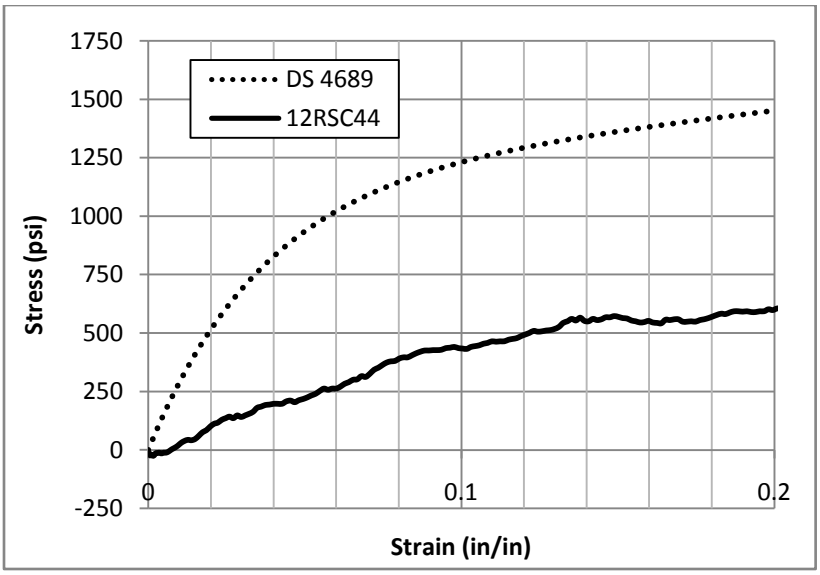

Figure C.2 .44/300 Ball Compared to the Viscoelastic Model

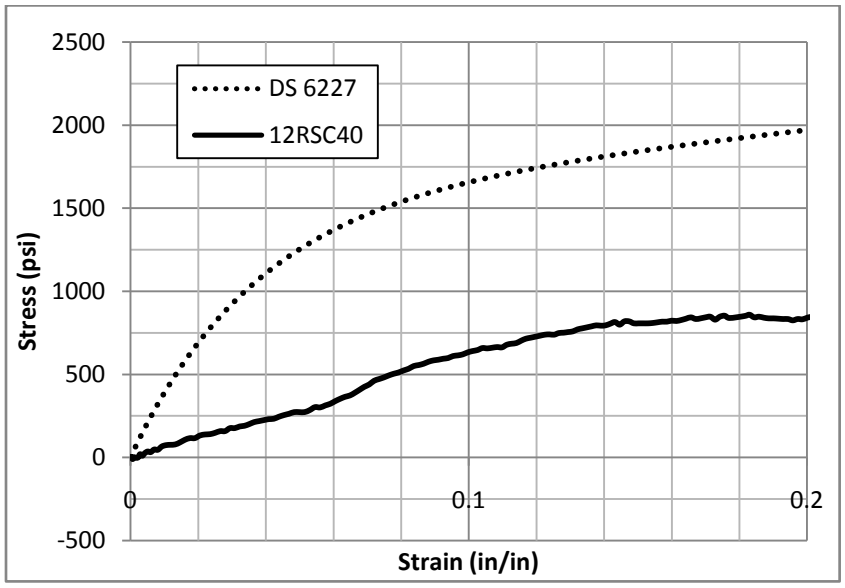

Figure C.3 .40/375 Ball Compared to the Viscoelastic Model

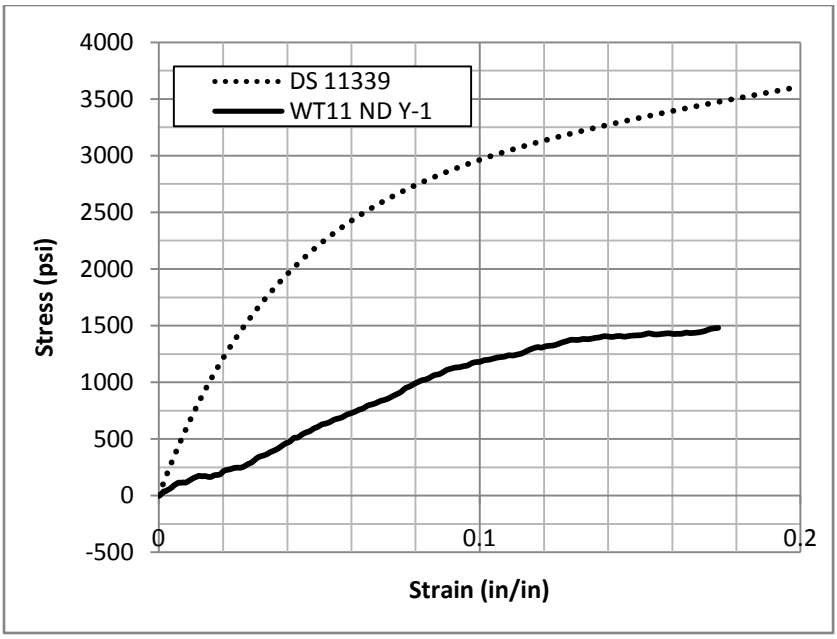

Figure C.4 .44/525 Ball Compared to the Viscoelastic Model